
Theses and Dissertations

Spring 2010

Quantitative analysis of retinal function in early stages of retinal degeneration in the rd1 mouse

Erik Lee Nylén
University of Iowa

Copyright 2010 Erik Lee Nylén

This thesis is available at Iowa Research Online: <http://ir.uiowa.edu/etd/565>

Recommended Citation

Nylén, Erik Lee. "Quantitative analysis of retinal function in early stages of retinal degeneration in the rd1 mouse." MS (Master of Science) thesis, University of Iowa, 2010.
<http://ir.uiowa.edu/etd/565>.

Follow this and additional works at: <http://ir.uiowa.edu/etd>



Part of the [Biomedical Engineering and Bioengineering Commons](#)

QUANTITATIVE ANALYSIS OF RETINAL FUNCTION IN EARLY STAGES OF
RETINAL DEGENERATION IN THE RD1 MOUSE

by
Erik Lee Nylén

A thesis submitted in partial fulfillment
of the requirements for the Master of
Science degree in Biomedical Engineering
in the Graduate College of
The University of Iowa

May 2010

Thesis Supervisor: Assistant Professor Steven F. Stasheff

Copyright by
ERIK LEE NYLEN
2010
All Rights Reserved

Graduate College
The University of Iowa
Iowa City, Iowa

CERTIFICATE OF APPROVAL

MASTER'S THESIS

This is to certify that the Master's thesis of

Erik Lee Nylén

has been approved by the Examining Committee
for the thesis requirement for the Master of Science
degree in Biomedical Engineering at the May 2010 graduation.

Thesis Committee:

Steven F. Stasheff, Thesis Supervisor

Edwin Dove

Chris Johnson

Joseph Reinhardt

Edwin Stone

In loving memory of

James Link Nylén

1949-2005

My greatest concern was what to call it. I thought of calling it ‘information,’ but the word was overly used, so I decided to call it ‘uncertainty.’ When I discussed it with John von Neumann, he had a better idea. Von Neumann told me, ‘You should call it entropy, for two reasons. In the first place your uncertainty function has been used in statistical mechanics under that name, so it already has a name. In the second place, and more important, nobody knows what entropy really is, so in a debate you will always have the advantage.’

Claude Shannon
Scientific American

ACKNOWLEDGMENTS

I thank Dr. Edwin Dove for serving as an outstanding adviser and providing me with much support since the first day I set foot on campus at Iowa. I give many thanks to Dr. William Scott, Melinda Skellenger, Dr. Thomas Oetting, and Dr. Richard Olson for providing me with the opportunity of involvement with Department of Ophthalmology & Visual Sciences.

I give thanks to Dr. Edwin Stone for being an influential mentor and providing me with encouragement and guidance at every step. I thank Dr. Chris Johnson for his support and advice, and Dr. Joe Reinhardt for his outstanding leadership in the Department of Biomedical Engineering and support of my work.

I give a special thanks to Dr. Steven Stasheff for his mentorship and support of this thesis, and the many conversations about science.

I thank Dr. Stewart Thompson and Dr. Tyson Kinnick for their mentorship and support of my personal and professional interests.

I give thanks to all members of the Stasheff Lab, Stone Lab, College of Engineering, and Departments of Ophthalmology & Visual Sciences and Pediatrics who have helped me at each juncture.

I thank all of my friends, notably those in Dance Marathon and ICHI, for much needed support over the years.

I give the highest acknowledgment to my brother, Paul, without whom I would have never accomplished any of this thesis, as well as Mom, Dad, my grandparents, cousins, aunts, and uncles, for their unwavering support of my every venture, no matter how far off the path it may seem.

ABSTRACT

In this thesis, I use a range of techniques in computational neuroscience, communication theory, and electrophysiology to characterize functional changes that occur in early stages of retinal degeneration in the mouse. At post natal day 14, retinal ganglion cells in the *rdl* mouse exhibit peculiar differences from age matched controls: an increased latency of responses to the onset of a light stimulus, decreased spike count in response to stimulus onset, increased spontaneous firing activity, and a decrease in information transmission. I propose this is due to an up-regulation of OFF bipolar cell excitation, a critical factor in functional changes seen in *rdl*, and use innovative techniques to discover findings that support these claims.

TABLE OF CONTENTS

LIST OF FIGURES.....	vii
LIST OF ABBREVIATIONS.....	viii
CHAPTER I: PERSPECTIVE.....	1
CHAPTER II: BACKGROUND	4
Structure and Function of the Eye.....	4
The <i>Rd1</i> Retina.....	11
Information Theory in Neural Coding.....	12
CHAPTER III: ELECTROPHYSIOLOGICAL TECHNIQUES.....	14
Tissue preparation.....	14
Multielectrode recording.....	14
Visual stimulation.....	15
Spike waveform analysis	16
CHAPTER IV: DYNAMIC RESPONSES IN DEGENERATION	19
Computational Methods.....	19
Results.....	20
Discussion	24
<i>Future Studies</i>	27
CHAPTER V: PARALLEL PATHWAYS IN THE RETINA.....	28
Computational Methods.....	28
Results.....	30
Discussion	33
<i>Future Studies</i>	38
CHAPTER VI: INFORMATION CAPACITY IN DEGENERATION.....	39
Computational Methods.....	39
Results.....	40
Discussion	42
<i>Future Studies</i>	46
CHAPTER VII: CONCLUSION.....	47
REFERENCES	48
APPENDIX: MATLAB DOCUMENTATION.....	55

LIST OF FIGURES

Figure

1.	Gross Structure of the Mouse Eye.....	5
2.	Cellular Structure of the Retina.....	6
3.	Model of Developing <i>wt</i> Retina	10
4.	Baseline Spontaneous Firing Rates	21
5.	Spike Count at Highest Stimulus	22
6.	Distribution of the Intensity-Response Profiles and Distribution of I_{50} Values in the <i>wt</i> P14 Retina.....	23
7.	Distribution of the Intensity-Response Profiles and I_{50} Values in the <i>rdl</i> P14 Retina.....	23
8.	Distribution of Slopes at I_{50}	24
9.	Model Depiction of Principle Functional Changes in the Dynamic Response Profile of the <i>rdl</i> Retina	26
10.	Response Dominance Indices	31
11.	Latency of ON Responses at Brightest Stimulus	32
12.	Transientness of Cellular Responses at Each Stimulus Intensity.....	32
13.	Off Latencies at Brightest Stimulus	33
14.	Proposed Model of <i>wt</i> Retina Compared to <i>rdl</i> Retina.....	37
15.	Naive Entropy Estimates	41
16.	Entropy of Noise	41
17.	Mutual Information Between Stimuli and Responses.	42

LIST OF ABBREVIATIONS

AC: Amacrine cell

BC: Bipolar cell

cGMP: Cyclic guanosine monophosphate

dLGN: Dorsal lateral geniculate nucleus of the thalamus

GCL: Ganglion cell layer

INL: Inner nuclear layer

IPLa: Inner plexiform layer sublamina *a*

IPLb: Inner plexiform layer sublamina *b*

ipRGC: Intrinsically photosensitive melanopsin containing retinal ganglion cell

MEA: Multi-electrode array

OFF-BC: Off bipolar cell

ON-BC: On bipolar cell

ONL: Outer nuclear layer

OPL: Outer plexiform layer

PDE: Phosphodiesterase

RD1: Retinal degeneration type 1

RGC: Retinal ganglion cell

Rod-BC: Rod bipolar cell

RPE: Retinal pigmented epithelium

WT: Wild type

CHAPTER I: PERSPECTIVE

In 1851, Herman von Helmholtz explored the optics of the eye and revolutionized medicine with the invention of the ophthalmoscope (Helmholtz, 1867). This simple tool allowed live observation of the retina, arguably spurring the development of ophthalmology as its own field worthy of study. Then in the early 1900s, Santiago Ramon y Cajal crafted a series of paintings detailing the intricate structures of the nervous system, including the cells of the retina (Berciano et al, 2001). This landmark work paved the way for what would become modern neuroscience. Advances in anatomical understanding of the brain followed, but it was not until 1952 that Alan Hodgkin and Andrew Huxley recorded electrical signals from the giant squid axon, showing that fundamental properties of neural communication could be explained by well established mathematical principles (Izhikevich, 2007). Seven years later, David Hubel and Torsten Wiesel applied these methods to the visual cortex (Hubel et al, 1959). People had known for ages that the eye was connected to the brain, but Hubel and Wiesel's findings were the first to effectively describe how the brain interprets information from the eye. These and other studies mark the advancement of a field known as "electrophysiology," the study of electrical phenomena in organisms.

In parallel with this progress in medicine and biology, physics and engineering were also rapidly advancing. Based on Nicolas Carnot's findings in the 1820s, the 1860s debate between the mathematicians Josiah Gibbs and Ludwig Boltzmann (among others) led to the principles of entropy and the second law of thermodynamics. At Bell Laboratories in 1948, Claude Shannon published *A Mathematical Theory of Communication*, revolutionizing digital communication by using the basic equation that

Gibbs had developed and applying it to electrical engineering (Shannon, 1948). This marked the beginning of what is known as "information theory." Within the following decades, physicists, engineers, and biologists began collaborations giving major insights into neural network theories, artificial intelligence, neuroscience, electrophysiology, and a multitude of other disciplines (Haykin, 1999). The work of the aforementioned figures and everyone in between provides an incredible foundation of knowledge upon which to build.

The goal of this manuscript is to propose a mechanism underlying signaling properties characteristic of the retinal degeneration mouse, and convince the reader that information theoretic methods can be useful for better understanding vision loss. The *rd1* mouse is a model of retinitis pigmentosa, an inherited blinding eye disease affecting approximately 1 in 4000 humans. Electrophysiological methods are used here to characterize retinal function in the *rd1* mouse, and information theory is applied to understand how changes in retinal function alter the utility of retinal responses to light in providing useful information. The broader implications of this approach are to better understand disease and ultimately find treatments in the fields of ophthalmology, neurology, and psychiatry.

Chapter II provides the reader with a background in basic biology and physiology of the adult, developing, and degenerate mouse retinas, followed by an introduction to concepts in information theory. **Chapter III** covers relevant techniques used in electrophysiology. In **Chapter IV**, I show how the dynamic responses of retinal ganglion cells are altered in degeneration. **Chapter V** presents potential mechanisms within the parallel pathways of the retina that might account for observations in disease.

In **Chapter VI**, I introduce information theoretic methods as a useful set of tools to quantify and explain disease mechanisms. **Chapter VII** concludes this thesis, followed by **References** and **Appendix**.

CHAPTER II: BACKGROUND

This chapter covers basic anatomy and physiology of the normal mouse retina. Relevant topics in retinal development and degeneration are introduced. It concludes with a brief introduction to quantitative techniques in analysis of retinal physiology.

Structure and Function of the Eye

The eye serves two major functions in mammals: spatial detection of light for image-forming vision, and irradiance detection to regulate acclimating responses in physiology and behavior (Foster, 2002). Despite the importance of both of these functions, much of the structure of the eye is specialized to the spatial detection of light for image-forming vision. In simple terms, the eye is a globe with optically refined anterior structures focusing light onto the retina covering the posterior inner surface of the eye (**Figure 1**).

The light sensitive retina is a highly structured complex of photoreceptors, neurons and support cells, with well-defined layers lining the back of the eye (**Figure 2**). Detection of light begins when opsin-photopigment in the photoreceptors absorbs a photon of light and initiates a chemical phototransduction cascade. In rods, photon absorption by 11-cis-retinal causes rhodopsin activation, in turn catalyzing the G protein transducin (Stryer 1996). The transducin activates a photodiesterase that hydrolyzes cGMP. The reduction in cytoplasmic cGMP concentration causes closure of cGMP-gated channels that in turn leads to a membrane hyperpolarization and reduction of glutamate release from the rods (Baylor et al, 1979). These initial stages of phototransduction in rods have been extensively characterized (for reviews, see Fu et al, 2007; Arshavsky et al, 2002).

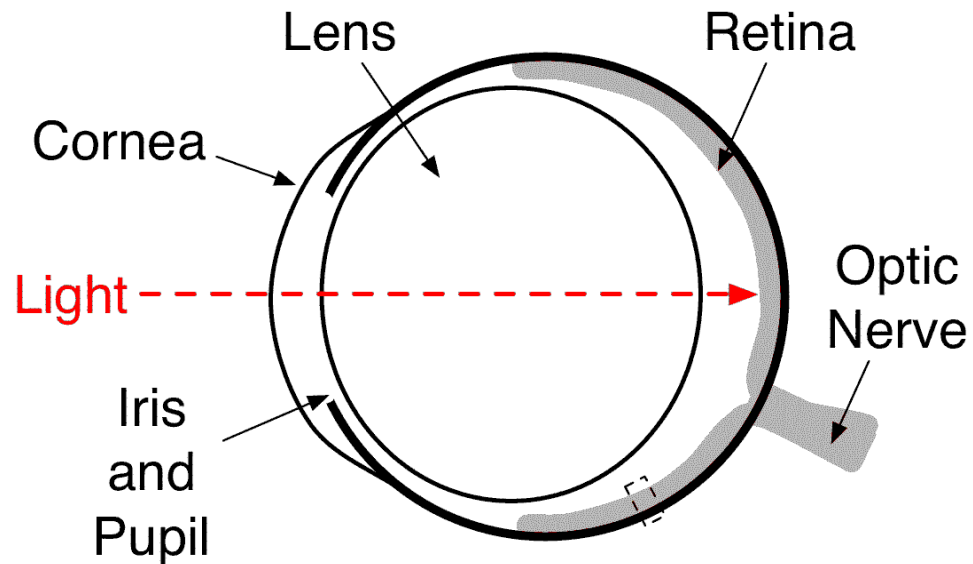


Figure 1. Gross Structure of the Mouse Eye. Note the mouse lens is large relative to the globe as compared to the lens in humans. Image courtesy Dr. Stewart Thompson.

The photoreceptors can be classified into two main groups, the rods and the cones. The ~6.4 million rods in the mouse are used for detecting dim or scotopic light levels and the ~0.2 million cones are used for detecting bright or photopic light levels (Jeon et al, 1998). Two main cone opsin types exist in the mouse, the short wave length S-cones optimally detecting light at 360nm, and the longer wavelength M cone tuned to detect 508 nm (Nikonov et al, 2006). However, many cones within the mouse retina express both the S and M opsin (Applebury et al, 2000).

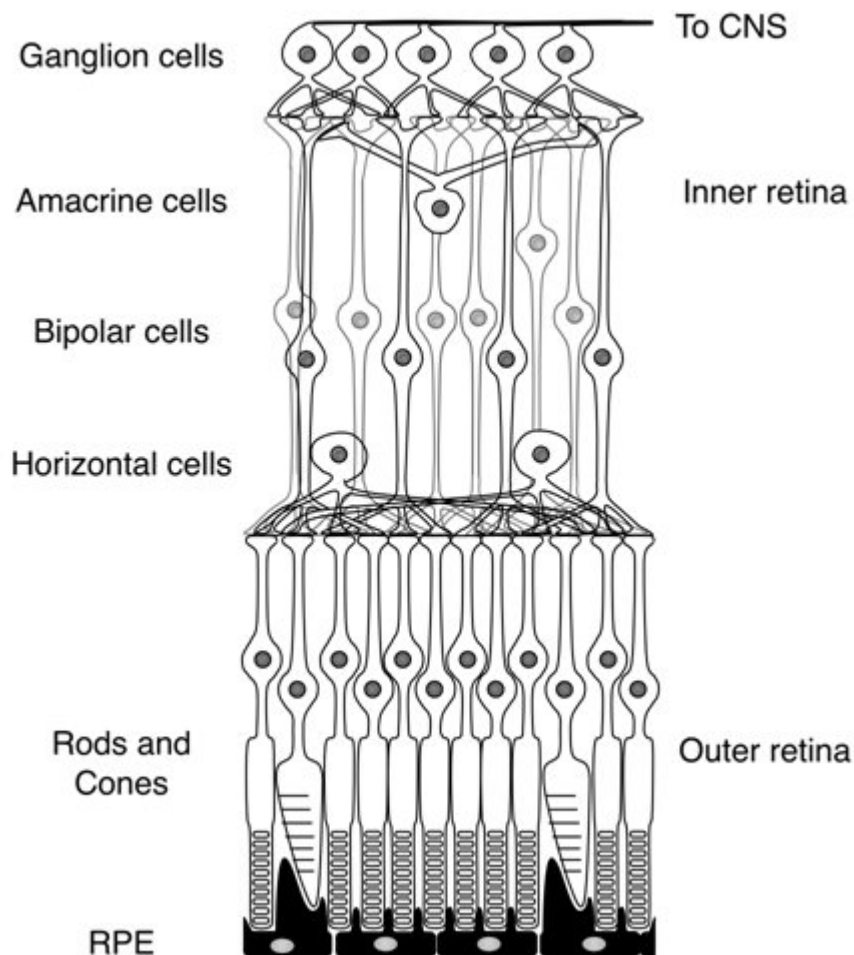


Figure 2. Cellular Structure of the Retina. Image courtesy Dr. Stewart Thompson.

Light-evoked reductions in glutamate release at the photoreceptor synapses generate a graded potential in bipolar cells (BCs) that express glutamate receptors (Marc, 1999). Cones connect two major types of cone bipolar cell: metabotropic receptor-expressing on depolarizing (to light) or ON-BCs, and ionotropic receptor-expressing on hyperpolarizing or OFF-BCs (Harveit, 1997). Each cone functionally synapses with at least one bipolar cell. Bipolar cells form a diverse mosaic arrangement, modify and pass

visual signals to other bipolar cells, amacrine cells and retinal ganglion cells (Han et al, 2005; Witkovsky, 2004; Wassle et al, 2009). The primary afferent pathway of rods is by rod-BCs that pass signals through AII-amacrine cells that then connect to cone ON-BCs and OFF-BCs. Rods also exhibit electrical coupling to cones, and synapse with cone OFF-BCs (Wu et al, 1988). Photoreceptors also connect to horizontal cells that provide synaptic feedback to both rods and cones at the level of the OPL, and can project feed-forward axons to the IPL (Thoreson et al, 2008). A high degree of cellular diversity further emphasizes the complexity in retinal signal propagation pathways, with upwards of ten functionally distinct bipolar cell types (Chan et al, 2001), over 30 amacrine cell types (MacNeil et al, 1998), and several types of horizontal cell.

The ~45,000 RGCs then receive glutamatergic inputs from amacrine cells and bipolar cells at the inner plexiform layer (IPL), some of which are electrically interconnected by gap junctions (Pan et al, 2010; Jeon et al, 1998). Ganglion cells can be generally grouped into three classes, those responding to the onset of light stimulus (ON-RGCs), those responding to the offset of light stimulus (OFF-RGCs), and those responding to either onset or offset of light stimulus (ON/OFF RGCs). Dendrites of OFF-RGCs typically stratify in the outer sublayer of the IPL, while ON-RGCs dendrites typically stratify in the inner layer of the IPL. As one might expect, ON-BCs typically synapse with ON-RGCs, while OFF-BCs typically synapse with OFF-RGCs, a nice example of serial signaling within a parallel dominant architecture. RGCs can be further categorized by other functional and morphological features into over ten groups - several subsets are extensively discussed below (Diao et al, 2004). Axons of RGCs converge to form the optic nerve and project to the visual centers of the brain such as the dorsal

lateral geniculate nucleus, and superior colliculus (Stevens et al, 1976). Non-visual centers of the brain are also connected by a special class of intrinsically photosensitive melanopsin-containing retinal ganglion cells (ipRGCs). These act in regulation of physiology and behavioral states such as sleep, as previously mentioned (Hattar, 2006). The retinal pigmented epithelium (RPE) and Mueller cells play a critical support function for the retina. The RPE supports the activity of the photoreceptors, regenerating the 11-*cis*-retinal necessary for opsin-photopigment, and reducing scatter of light within the eye. Muller cells also span the layers of retina, primarily acting as non-signaling glial cells in maintaining the health and form of other retinal cells.

The action potentials of retinal ganglion cells, the final step in signal propagation from the retina, colloquially known as "spikes," are binary messages whose temporal arrangement are the basis of this study.

Development of the *Wild Type* Mouse Retina

At birth, the visual system is far from mature. A large number of activity independent developmental processes occur in prenatal neural retina (for reviews, see Lambda et al, 2008; and Mu et al, 2008). However, the activity dependent maturation of the retina is a major focus of this thesis. In particular, the balance of spontaneous activity and light driven activity is investigated.

After birth and before eye opening (P0-P12), "retinal waves" are observed (Wong, 1999). These waves are light-independent bursts of activity in RGCs triggered by acetylcholine release from starburst amacrine cells (Masland, 1977). Such waves radially propagate via gap junctions in the GCL about a finite area determined by the RGC density (Firth et al, 2005). Retinal ganglion cells activated during these waves transmit

temporally and spatially correlated clusters of spikes to the dLGN (Wong, 1999). This is a necessary step in proper lamination of higher visual relay stations (Shatz, 1996). For instance, synaptic blockade of sodium channels at the RGC/dLGN synapse disrupts ocular dominance column segregation in the cortex (Stryker et al, 1986). A similar effect on cortical development is generated when animals are raised under strobe lights that synchronize binocular activity (Schmidt et al, 1985). This balance in activity underscores the need for monocular correlated activity in development of the retinogeniculate pathway.

Synaptic activity also drives dendritic stratification within the inner plexiform layer. Just before eye opening, the majority of RGCs exhibit both ON and OFF response characteristics, but in the adult mouse retina, less RGCs are considered ON/OFF (Sernagor et al, 2001; Volgyi et al, 2004). This high proportion of single RGCs with both ON and OFF responses is due to diffuse stratification of RGC dendrites in the IPL (Tian et al, 2003). Just after eye opening, RGCs exhibit many more dendritic spines than in adult (Diao et al, 2003). Pathway specific segregation of signals from the INL involves "pruning" of these dendrites in the IPL (Tian et al, 2003). Raising animals in the dark or blocking glutamate transmission in the developing retina halts the maturation of dendritic specification (Bisti et al, 1998). This indicates the need for light evoked synaptic activity for the proper lamination of the IPL. Basic structure and function in the *wt* P14 retina is depicted in **Figure 3**.

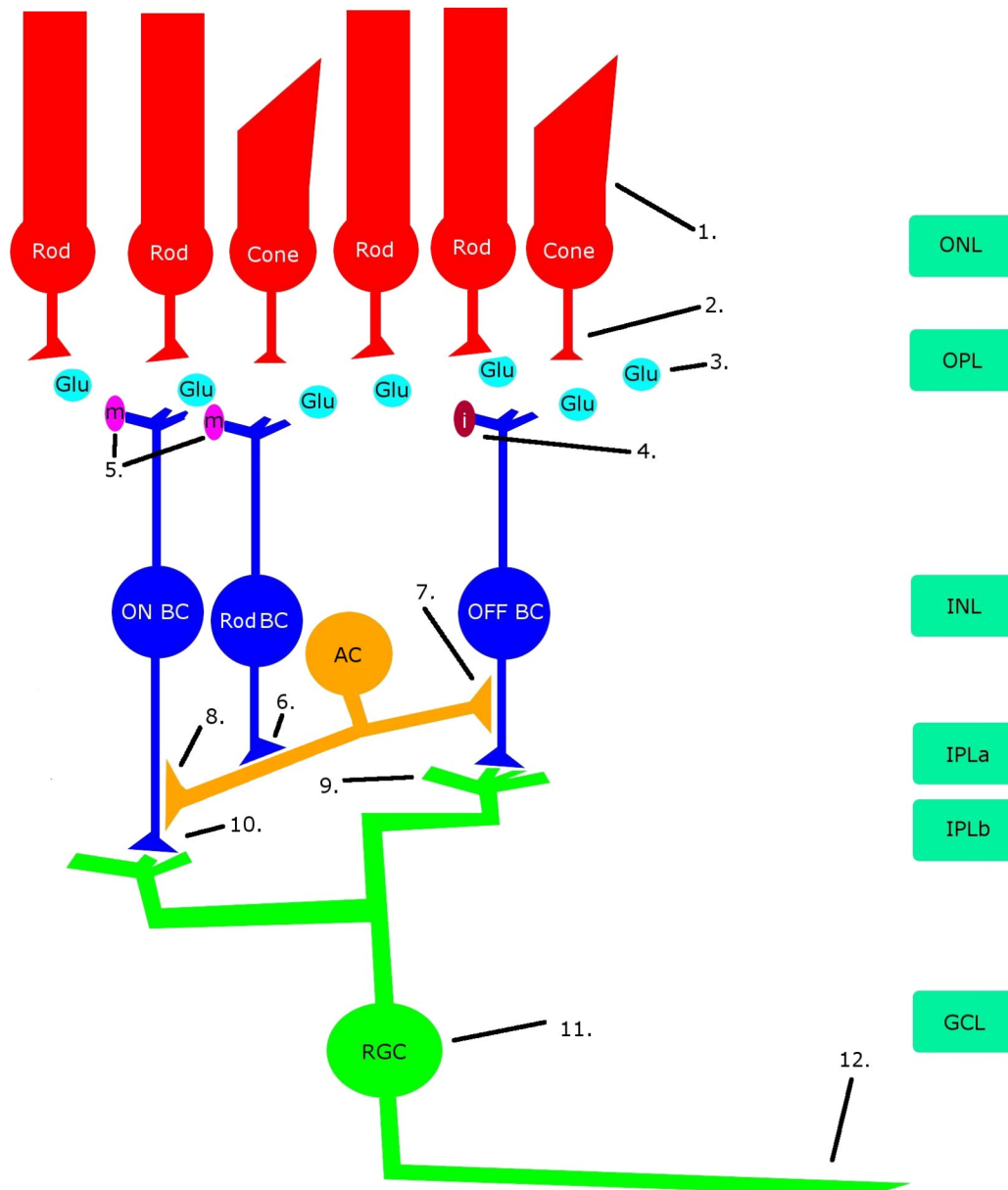


Figure 3. Model of Developing *wt* Retina. (1) Light is absorbed in the photoreceptors. Phototransduction within the inner segments causes a hyperpolarization of the cell. (2) Upon hyperpolarization, glutamate release from the rod spherules and cone pedicles decreases. (3) Decreased glutamate release from the photoreceptors results in decreased glutamate concentration in the outer plexiform layer. (4) Ionotropic receptors are deactivated when glutamate concentration falls. Note that these receptors cause graded depolarizing potential signals in the OFF-BCs in the presence of glutamate. (5) Decreased glutamate concentration decreases activation of the metabotropic glutamate receptors. Activation of these receptors causes a graded potential change in ON-BC soma. Thus, in the ON-BCs, a sign-inverting depolarization occurs at light onset. (6) Rod BCs synapse with ACs, which transmit signals to ON BCs. (7) Activation of the OFF-

Figure 3—continued BC causes amacrine cells to high pass filter and suppress signals in the ON-BCs at light offset. (7) As OFF-BCs are deactivated with light onset, the amacrine cell mediated suppression decreases. Likewise, ON-BC signals suppress the OFF pathway through a similar amacrine mediated mechanism. (8) OFF-BCs synapse with RGCs in IPLa, transmitting signals with glutamate. (9) ON-BCs synapse with RGCs in IPLb, signaling via glutamatergic activation. Retinal ganglion cells integrate signals from both (8) and (9) within the dendrites and soma (11). Spikes are generated at the initial segment of the axon in the RGCs and transmitted via the axons to the brain (12). Abbreviations: AC, amacrine cell; Glu, glutamate; i, ionotropic glutamate receptor; INL, inner nuclear layer; IPLa, inner plexiform layer sublamina *a*; IPLb, inner plexiform layer sublamina *b*; m, metabotropic glutamate receptor; OFF-BC, off cone bipolar cell; ON-BC, on cone bipolar cell; ONL, outer nuclear layer; PhR, photoreceptor; RGC, retinal ganglion cell; Rod BC, rod bipolar cell. Note: horizontal and Muller cells not included in figure.

The *Rdl* Retina

The retinal degeneration mouse (*rdl*, historically known as *rd*) has been a great resource for studies of inherited retinal disease for over 80 years (Keeler, 1924). The abnormality stems from a nonsense mutation in the 7th exon of *PDE6B* (Bowes et al, 1990). This gene encodes cGMP-phosphodiesterase in rods, an essential protein in the phototransduction cascade. Mutations in *PDE6B* in humans commonly cause retinitis pigmentosa (RP), a class of blinding eye diseases (Phelan et al, 2000). Like various subtypes of RP, loss of vision occurs early in *rdl*. At P8, electroretinographic responses and histology both appear normal compared to age matched controls (Farber et al, 1994). Activity levels of the metabotropic glutamate receptors and bipolar cells appear normal. The loss of rods is believed to begin at P10, with peak degeneration at P14 (Sancho-Pelluz et al, 2008). By P14, there is reduced photoreceptor layer thickness, and pronounced horizontal cell axon sprouting (Strettoi et al, 2002). An increase in spontaneous hyperactivity of the RGCs occurs at this age. Death of rod cells is essentially complete by P21, with no recordable electroretinogram by P28. Secondary

loss of cones occurs in parallel but is more protracted and residual cone cell bodies can exist for several weeks thereafter (LaVail et al, 1997). By P60, an increased level of activity is observed in the RGCs despite complete loss of response to light stimulation (Stasheff, 2008). At P90, near complete loss of Rod-BC dendrites is observed, with no apparent morphological changes in amacrine cells (Strettoi et al, 2002). Significant remodeling of inner neural circuitry occurs after this date (Marc et al, 2003).

The precise mechanism and cause of photoreceptor cell death, by apoptotic, necrotic, or other means, is an actively studied area (Portera-Cailliau et al, 1994; Hackam et al, 2004; Sancho-Pelluz et al, 2008). It has been suggested that overabundance of free glutamate in the retina contributes to degeneration (Lucas et al, 1957). In early stages of *rd1*, administration of a glutamate receptor antagonist significantly reduces morphological changes associated with degeneration, supporting a glutamate-toxicity hypothesis (Delyfer et al, 2005; Olney, 1969).

Information Theory in Neural Coding

In 1948, Claude Shannon published a seminal paper, *A Mathematical Theory of Communication*, proposing the use of entropy as a measure of information capacity in communication systems. At this point in time, entropy had already been established as a useful tool in thermodynamics (Carroll, 2010). Classically, entropy was a measure of variance or disorder in a physical system. The second law of thermodynamics states that the entropy of a macroscopic system can never decrease. Shannon capitalized on the statistical power of this measure and expanded it to communication theory. "Shannon entropy" quantifies the amount of information in a message (Rieke et al, 1997). Entropy has since been a powerful measure in statistical mechanics and neural coding (Jaynes,

1957; Rieke et al, 1997; Strong et al, 1998). Other applications of entropic measures include climate prediction and cosmology (Ruddell et al, 2009; Carroll, 2010). For the purposes of this thesis, "entropy" refers to Shannon entropy.

Information theory is applied here in understanding how much "useful" vision exists in early stages of retinal degeneration. Calculations of retinal ganglion cell information rate range between 20-70 bits per second (Passaglia et al, 2004). Such estimates are dependent on linear decoding methods, which are discussed below. As previously noted, an increased level of noise occurs in the *rdl* mouse. This noise introduces an additional level of uncertainty in the spike train analysis (Passaglia et al, 2004; Sterling et al, 2007). Thus, this thesis emphasizes the use of well established methods in spike train characterization. Information theoretic techniques are used to further explain functional changes in the diseased retina.

CHAPTER III: ELECTROPHYSIOLOGICAL TECHNIQUES

Tissue preparation

Wild-type (C57BL/6J strain) and *rd1* mice (B6.C3-*Pde6b*^{rd1} *Hps4*^{le}/J or a C3H/HeJ strain) were bred within a local colony established from purchased breeding pairs (Jackson Laboratories, Bar Harbor, ME). Animals were cared for in accordance with institutional guidelines of the University of Iowa Institutional Animal Care and Use Committee. Animals were dark-adapted for ≥ 30 min prior to being anesthetized with intraperitoneal or intramuscular injection of xylazine (10-40 mg/kg) and ketamine (50–200 mg/kg) sufficient to extinguish tail pinch and corneal reflexes. Under infrared illumination to minimize exposure to visible light, using a dissecting microscope (Leica Microsystems, Bannockburn, IL) with infrared image intensifiers (BE Myers, Redman, WA), the retina was dissected from the retinal pigmentary epithelium, placed ganglion cell layer down onto a multielectrode recording array (10 μm contacts spaced 200 μm apart; Multichannel Systems, Reutlingen, Germany), and perfused with warm (36–37°C), oxygenated Ringer medium at a rate of 2.5–4 ml/min (Meister et al. 1994; Tian and Copenhagen 2001). Ringer medium included (in mM) 124 NaCl, 2.5 KCl, 2 CaCl₂, 2 MgCl₂, 1.25 NaH₂PO₂, 26 NaHCO₃, and 22 glucose.

Presented data are from a total of 311 *wt* cells from 6 retinas, and 315 *rd1* cells from 4 retinas.

Multielectrode recording

A 60-channel amplifier (Multichannel Systems, Reutlingen, Germany) mounted on a microscope stage (Zeiss Axioplan, Göttingen, Germany) interfaced with digital sampling hardware and software (Bionic Technologies, Salt Lake City, UT) for recording

and analyzing spike trains from each of the electrodes in the array. Digitized data initially were streamed onto the computer's hard drive and further analyzed off-line. After transfer of the retina to the recording chamber, recordings were allowed to stabilize for ≥ 1 h as evidenced by stable action potential amplitudes, number of cells recorded, frequency of spontaneous firing, and consistency of light-evoked responses (where obtainable). Twenty-minute epochs of continuous recording were obtained from typically 30–90 ganglion cells per retina at various intervals over several hours. Data presented are from the first 1–3 h of recording, unless otherwise specified.

Visual stimulation

In experiments with light stimulation, a miniature computer monitor (Lucivid, MicroBrightField, Colchester, VT) projected visual stimuli through a 5x objective, and these were focused via standard microscope optics (Zeiss Axioplan) onto the photoreceptor layer of the retina. Luminance was calibrated via commercial software (VisionWorks, Vision Research Graphics, Durham, NH), using a radiometer (Photo Research, Chatsworth, CA) and photodiode (Hamamatsu S1133-11, Hamamatsu City, Japan) placed in the tissue plane. The refresh rate of the monitor (66 Hz) was selected to avoid entrainment of retinal ganglion cells that might contaminate light responses (Tremain et al, 1983; Wollman et al, 1995). The same software controlled and recorded stimulus parameters, passing synchronization pulses to the data acquisition computer via a parallel interface with roughly 10 microsecond precision. Full field flash stimuli (retinal irradiance: 0–35 $\mu\text{W}/\text{cm}^2$, 1000 ms, P43 phosphor with peak emission at 545 nm) extended beyond the dimensions of the recording array (stimuli: 2,100 x 2,800 μm ; array: 1,700 x 1,700 μm) and were displayed at five second intervals. These parameters are

known to evoke a reliable ERG response and to allow separation of ON- and OFF-pathway responses in individual ganglion cells (Balkema et al, 1982; Stone et al, 1993; Strettoi et al, 2002). Responses were averaged over 10 or 20 trials.

Spike waveform analysis

Action potential (spike) waveforms accepted for further analysis were $\geq 60 \mu\text{V}$ in amplitude, and > 1.85 times the RMS of the background signal. To distinguish responses from different cells that might appear on the same electrode, a component of the data-acquisition software (Bionic Technologies) or a similar freeware (PowerNAP, Neuroshare, <http://neuroshare.sourceforge.net/index.shtml>) was used for supervised automated sorting of action potential profiles according to a principle components analysis (PCA) paradigm. For each electrode, the software displays a random sample of spike waveforms along with all the two-dimensional projections of each waveform in the space defined by the first three principle components (PCs, or eigen vectors computed from the correlation matrix for this data subset) (Wheeler 1999).

Individual waveforms were partitioned iteratively into one to five clusters according to an automated K-means or T-distribution paradigm (Wheeler 1999). In cases where an optimal solution was not immediately distinguished on this basis, the data initially was segregated into a greater number of clusters than seemed the likely final solution, for subsequent analysis of the corresponding spike trains (described in the following text), to determine which of these signals were generated by the same or distinct sources. The mean waveform for each of the clusters was displayed; if these mean waveforms appeared nearly identical among two or more clusters, these were joined manually. The mean waveform for each of the clusters chosen at this stage served

as a series of templates, and all remaining waveforms from that electrode were joined by the software to the cluster closest to it in PC space.

Appropriate assignment of individual waveforms to distinct cells was confirmed further by analysis of the corresponding spike trains. Interspike interval (ISI) histograms were computed for each spike train by measuring the intervals between spikes in the train for all possible spike pairs, then distributing these values in bins of 0.2-ms width. ISI histograms from accepted data demonstrated a refractory period of >1 ms (typically 2–5 ms) and did not reflect any of several patterns of recognizable noise: 60 Hz, very high-frequency (>10 kHz) transients, or waveforms distinct from those of extracellular action potentials (e.g., sinusoidal oscillations). Cross-correlograms were computed in like fashion, measuring all intervals between each spike in one train and all spikes of the other train, binning at 5 ms. In cases where two or more templates from the same electrode appeared similar, the waveform clusters ultimately were assigned pair-wise to either one or two cells, based on their separate and combined ISI histograms and the cross-correlogram between their spike trains. Thus if the ISI histograms from the two putative cells were of clearly distinct shape, and/or if the ISI histogram formed by combining the two spike trains eliminated the refractory period observed in either separate ISI histogram, these spike trains were considered to have originated from two separate cells (Segev et al, 2004). Likewise if a prominent peak was observed near the origin in the cross-correlogram of the two spike trains, these spikes must have originated from two separate cells because both were recorded nearly simultaneously on the same electrode. These procedures generally resulted in one to three (occasionally four or five) cells being isolated from a single electrode.

The experimental methods described here were performed in the laboratory of Dr. Steven Stasheff, as published (Stasheff, 2008).

CHAPTER IV: DYNAMIC RESPONSES IN DEGENERATION

In this chapter I present the physiologic spike timing characteristics seen in retinal degeneration. Features of *rd1* mouse retinal ganglion cells include increased spontaneous activity, decreased spike output in response to bright stimuli, and shift in dynamic response profiles. I argue that these observations are in part due to an increase in glutamate concentration up-regulating the OFF pathway, and a decrease in photoreceptor cell count.

Computational Methods

The baseline spontaneous spike firing rate is the sum of all spikes occurring during periods not within 3000 milliseconds of a light stimulus (**Equation A**),

$$rate_{spont} = \sum_{t=L_{ON}}^{L_{OFF}} s_t \mid I_L = 0 \quad (\text{Equation A})$$

where s_t is the number of spikes occurring in timebin t , L_{OFF} is the time of light offset, L_{ON} is the time of light onset, and I_L is the relative intensity of the stimulus.

To deduce further cellular response characteristics, each cell's response to increasing intensities of light stimulus was constructed. These curves were fit with three functions. A general sigmoid function, Hill function, and cumulative Weibull function were tested for goodness of fit in each cell using the *mean square error* of the **nlinfit** function in MATLAB (See **Appendix**; Wallisch et al, 2009; Dayan and Abbott, 2001; Alon, 2007). The general sigmoid function gave the least error for the greatest number of

cells in any model fit. This subsequently was used to model each cell's responses to increasing stimulus intensity (**Equation B**).

$$R = \frac{R_{\max}}{1 + e^{-a \cdot I_L + I_{50}}} \quad (\text{Equation B})$$

R_{\max} is the cell's total spike count, I_{50} is stimulus intensity at which the cell exhibits 50% firing of its maximum response, a is the slope of the curve at I_{50} , and I_L is the intensity of any given stimulus. This yields a response R , which is linearly normalized to a maximum value of 1.

Results

Consistent with previous findings, *rdl* P14 retinal ganglion cells exhibit a significantly increased level of spontaneous activity compared to *wt* cells of the same age (**Figure 4**). At the highest stimulus intensity, the *wt* P14 cells show a significant increase in spike count compared to both *rdl* and adult (**Figure 5**). At P14 in the *rdl* mouse, the rate of photoreceptor degeneration is at its peak. These data indicate a decreased ON response, and less signal throughput in the INL in *rdl* than in *wt*.

Wild Type retinal ganglion cells exhibited a spectrum of responses to light stimulation for increasing intensities (**Figure 6**). The I_{50} value indicates the luminance at which a retinal ganglion cell fires 50% of its maximal spikes. A low I_{50} value indicates that a cell fires half of its maximal response at low luminance. These would be considered highly sensitive cells, since they respond to small amounts of light. These

cells are also said to “saturate” at low light levels. Responses of lower sensitivity cells do not saturate at the lower intensities, instead showing higher I_{50} values.

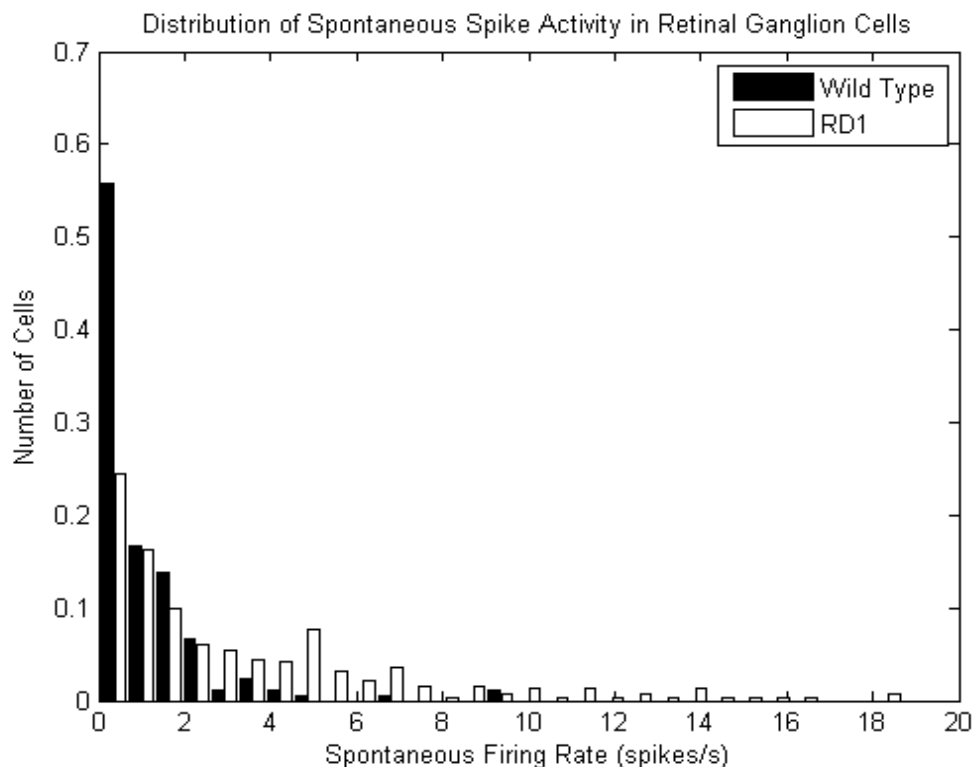


Figure 4. Baseline Spontaneous Firing Rates†. Under no light stimulus, the *rdl* P14 cells exhibit a significantly increased level of spontaneous activity (using **Equation F**) compared to *wt* cells of the same age ($p < 10^{-12}$, Kruskal-Wallis; Daniel, 2005). The increased level of free glutamate within the OPL is likely a factor in this distribution shift, as discussed below.

†NB: in bar graphs, bars between different cell types have been paired with each other for visualization purposes only. A white bar appearing adjacent to a black bar represents data from the same bin value.

Some *rdl* cells exhibit saturation at a dim light level, as indicated by the peak of cells at low I_{50} (**Figure 7**). These data indicate that this group of cells is incapable of responding over a wider dynamic range. To further evaluate the dynamic response

characteristics of these cells, the slopes of the cells at I_{50} were calculated. Comparing the slopes of these cells at I_{50} , *rd1* shows that more cells

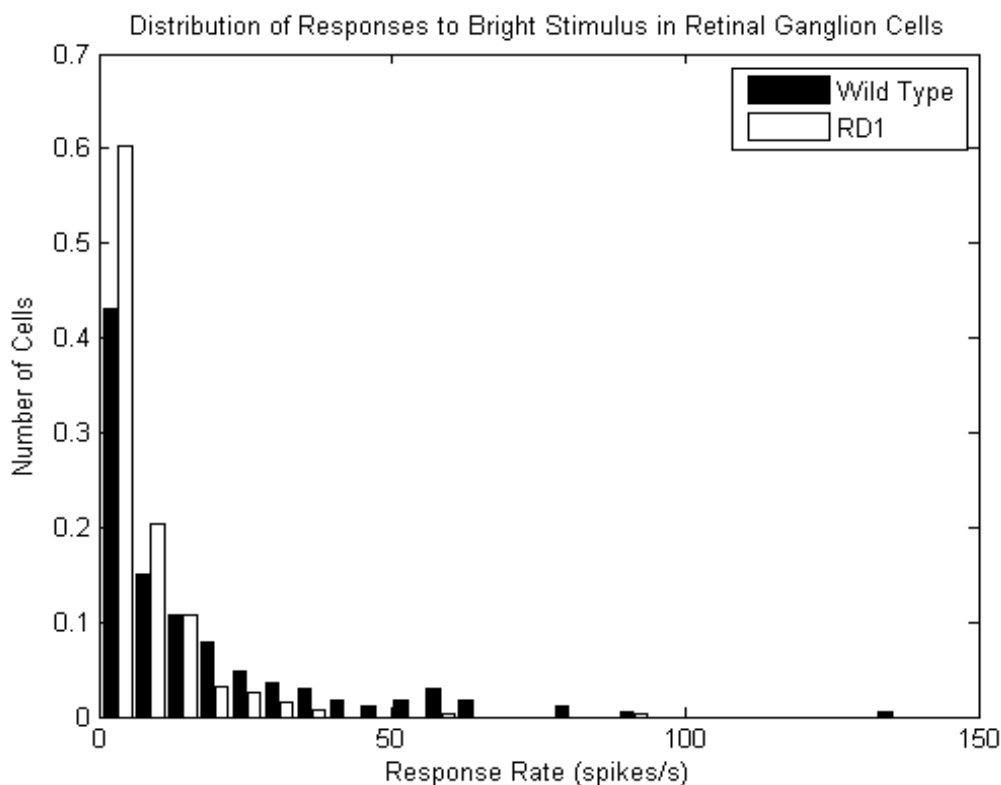


Figure 5. Spike Count at Highest Stimulus. The *rd1* P14 shows a significant decrease in spike count at the highest stimulus intensity *wt* ($p < 10^{-8}$, Kruskal-Wallis; Daniel, 2005). The *rd1* P14 and *wt* adult cells (not shown) exhibit no significant difference in spike count at brightest stimulus ($p = 0.19$).

exhibit higher slopes at I_{50} (**Figure 8**). This increased slope is indicative of greater sensitivity, and a narrower dynamic response range. The need for a dynamic response is discussed below, and possible mechanisms for this loss of range in response are discussed in subsequent chapters.

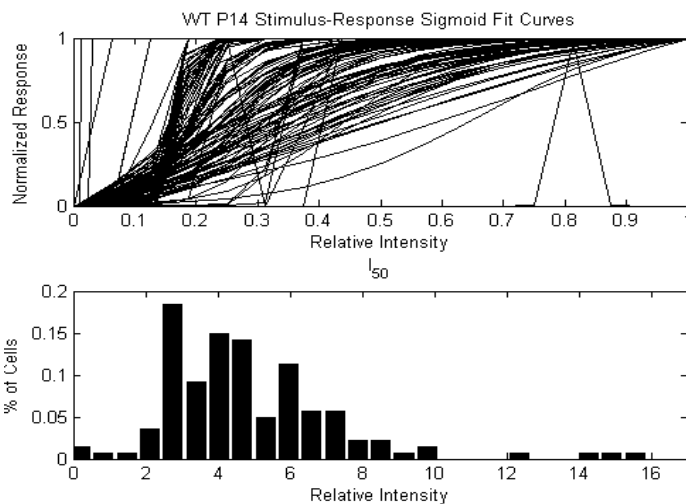


Figure 6. Distribution of the Intensity-Response Profiles and Distribution of I_{50} Values in the *wt* P14 Retina. Shown on top are the responses of all *wt* cells to increasing intensity full field stimuli. Below are the intensities at which 50% of each cell's maximum firing response is observed. Retinal ganglion cells exhibit a functional spectrum of response to stimulation across luminance intensities.

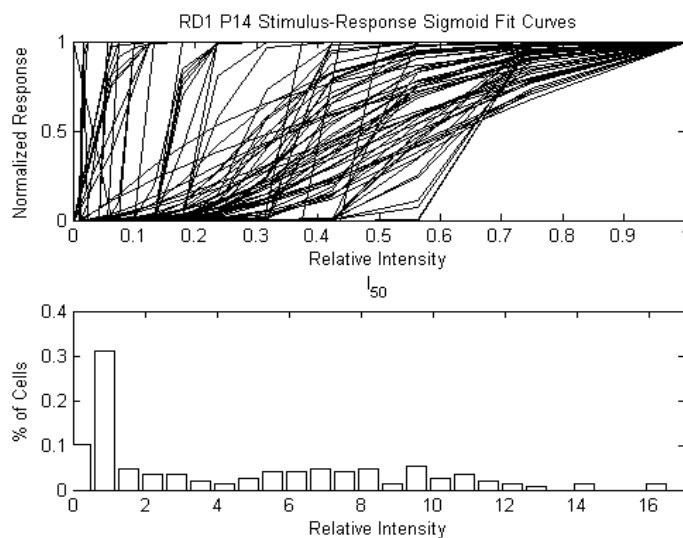


Figure 7. Distribution of the Intensity-Response Profiles and I_{50} Values in the *rd1* P14 Retina. A shift in I_{50} distribution is seen compared to the *wt* profiles.

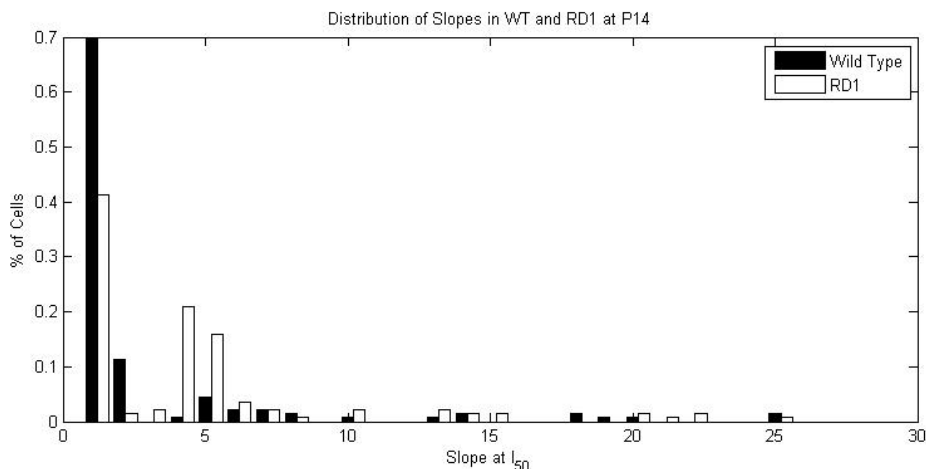


Figure 8. Distribution of Slopes at I_{50} . An increased number of cells with higher slopes are observed in the *rdl* cells ($p < 10^{-9}$, Kruskal-Wallis; Daniel, 2005).

Discussion

Noise can be a problem. Webster's Third New International Unabridged Dictionary first definition of noise is "loud, confused, or senseless shouting or outcry." The importance of this first definition becomes clear in the discussion on information theory below. Perhaps Webster's second definition is better suited though, "an unwanted signal that enters an electronic communication system (as telephone, radio, television) or that is created in it and that tends to interfere with the desired signals." Noise in the retina can be defined as any spiking activity that corrupts useful information transfer. As with telecommunications, if the noise is small compared to the signal, then a useful message can be identified. One can still watch a television show with small amounts of "snow" on the screen. However, if noise begins to outweigh the signal, useful message transmission declines.

Identifying noise in neural systems is no trivial task (Wilson et al, 1988; Passaglia et al, 2004). It is difficult to know which spikes from a hyperactive cell constitute noise

and which represent an accurate response. Thresholded systems often utilize noise to aid in transduction of weakly coded periodic signals. This is a phenomenon commonly known as stochastic resonance (Rousseau et al, 2003). It is tempting to speculate that the increased spike count in young wild type retinal ganglion cells as compared to adult cells (**Figure 5**) is a form of stochastic resonance, but this claim lacks supporting evidence. In this thesis, spontaneous spiking activity is considered to be noise.

What causes these functional changes observed in retinal degeneration? As mentioned previously, the *rdl* retina by age P14 has lost a large number of rod photoreceptors (Sancho-Pelluz et al, 2008), and spontaneous firing has increased (**Figure 4**). The remaining rods show much less function than their *wt* counterparts, leaving cones as the primary sensors of light in the retina. Recall that cones comprise less than three percent of photoreceptors in the mouse. This indicates reduced cellular signaling from the photoreceptor layer, perhaps contributing to the reduced spike count seen in **Figure 5**. Increased levels of glutamate are also present in the outer plexiform layer in *rdl*. Since photoreceptors transduce light onset by reducing glutamate output, the already low number of cones must compete with an increased glutamate concentration to cue the ON-BCs. Note that the ionotropic glutamate receptors of the OFF-BCs depolarize as a consequence of glutamate binding. This indicates the possibility of hyper-activation of iGluRs through increased glutamate levels. **Figure 7** indicates a peak in cells with an I_{50} value at low intensity stimulus. **Figure 8** depicts a change in the slopes of cells at each I_{50} . This can be described as an alteration in the dynamic response profile of *rdl* cells. Implications of these alterations and a possible mechanism to describe these are presented

below. The basic physiologic differences in *rd1* cells shown in this chapter are illustrated in **Figure 9**.

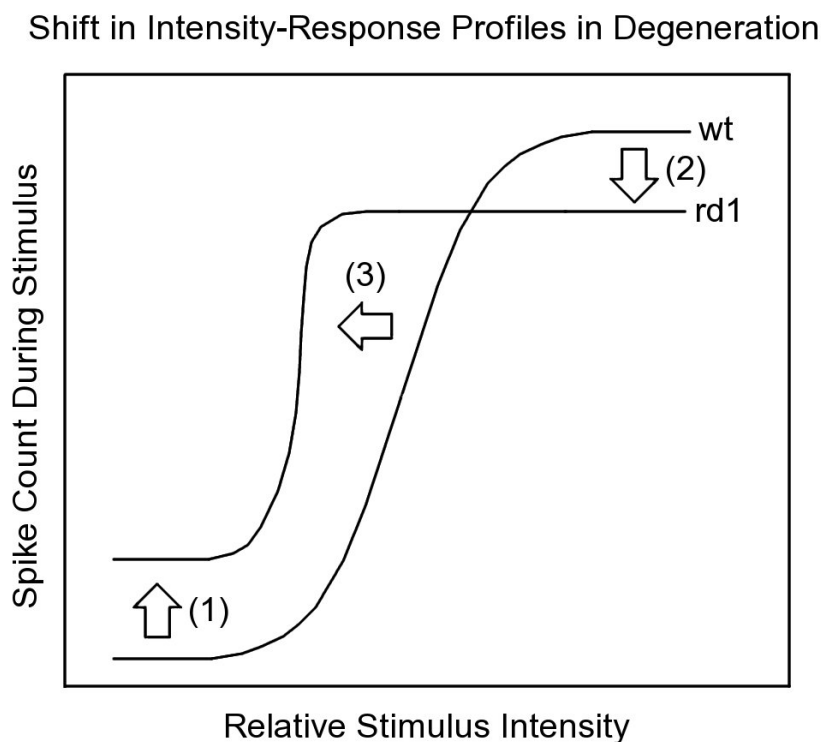


Figure 9. Model Depiction of Principle Functional Changes in the Dynamic Response Profile of the *rd1* Retina. In this drawing, the sigmoid curves represent the amount of spiking observed in retinal ganglion cells in response to increasing luminance levels of light stimulus. The baseline firing rate, or spontaneous activity, is increased in *rd1* (1). Spiking at the brightest stimulus level is reduced in *rd1* (2). The I_{50} exhibits a shift, as well as an increased slope (3).

Why does the retina need a wide dynamic range in neurons and have highly sensitive retinal ganglion cells? Metabolic efficiency and survival cost may be two reasons. Computationally, a neuron with a wide dynamic response requires much energy to faithfully respond to a widely dynamic input. At some level, the retina must sacrifice how much it can respond to with how much response is needed (Balasubramanian et al,

2002). High sensitivity neurons may be of key importance for survival, for instance, motion detection is useful for identifying potential predators. Downstream neurons may care less about message content than they care about message presence. For example, a subset of retinal ganglion cells have been shown to optimally respond to approaching objects (Munch et al, 2009). Preservation of highly sensitive pathways in disease might indicate an attempt to preserve basic survival tools. If there were one pathway that could be preserved in the course of disease, a preference for high sensitivity pathways may provide a brief window of vision for survival of young animals.

In the next chapter, I propose a mechanism to further explain the altered dynamic properties in retinal degeneration.

Future Studies

One could use pharmacological inhibition of the OFF-BC iGluRs to elucidate the role of glutamate in spontaneous activity in degeneration, though iGluRs are observed in many cell types of the retina, so specific targeting of the OFF pathway may be difficult. Inhibition of glutamate reuptake in the *wild type* retina could show how excess glutamate influences intraretinal signaling. To test for the preservation of basic survival tools in disease, one could test young *rd1* mouse behavior in response to images such as predators or food to elucidate the utility of the little vision that exists early in disease.

CHAPTER V: PARALLEL PATHWAYS IN THE RETINA

In this chapter, I present evidence for the role of the amacrine cell network in regulating spiking in retinal degeneration. I build on the findings in the previous chapter, using the observations of increased noise and decreased spike output to further hypothesis a mechanism that explains changes in latency and gain of the retinal ganglion cells. It is my goal to convince the reader that increased OFF bipolar cell activation causes increased amacrine cell filtering of the ON bipolar cells.

Computational Methods

Several values were calculated for each cell based on spike times. The proportionality of a cell's response is defined as the response to the onset of light compared to the response to both onset and offset of light (**Equation C**),

$$proportion_{ON} = \frac{\sum_{t=L_{ON}}^{L_{OFF}} s_t}{\sum_{t=L_{ON}}^{L_{OFF}} s_t + \sum_{t=L_{OFF}}^{2*L_{OFF}-L_{ON}} s_t} \quad (\text{Equation C})$$

where s_t is the number of spikes occurring in timebin t , L_{OFF} is the time of light offset, L_{ON} is the time of light onset, and I_L is the relative intensity of the stimulus. The complement of this value is easily calculated (**Equation D**).

$$proportion_{OFF} = 1 - proportion_{ON} \quad (\text{Equation D})$$

The Response Dominance Index is defined as the greater value between $proportion_{ON}$ and $proportion_{OFF}$ (**Equation E**).

$$response_{index} = \max(proportion_{ON}; proportion_{OFF}) \quad (\text{Equation E})$$

The transientness of the cell is determined by the fraction of a cell's response occurring in the first 200 milliseconds after the stimulus onset or offset, giving $transientness_{ON}$, and $transientness_{OFF}$ (**Equations F, G**),

$$transientness_{ON} = \frac{\sum_{t=L_{ON}}^{220+L_{ON}} S_t}{\sum_{t=L_{ON}}^{L_{OFF}} S_t} \quad (\text{Equation F})$$

$$transientness_{OFF} = \frac{\sum_{t=L_{OFF}}^{220+L_{OFF}} S_t}{2 * L_{OFF} - L_{ON} - \sum_{t=L_{OFF}} S_t} \quad (\text{Equation G})$$

where s_t is the number of spikes occurring in timebin t , 220 indicates the period of a transient response (in milliseconds), L_{OFF} is the time of light offset, and L_{ON} is the time of light onset.

The latency of the ON response is defined as the time between the stimulus onset and the peak response between stimulus onset and offset (**Equation H**). This value was

selected given the difficulty in approximated interpolated values. The latency of the OFF response is determined by the time between the stimulus offset and the peak response between stimulus offset and twice the stimulus duration thereafter (**Equation I**).

$$latency_{ON} = \max(s_t) | t = L_{ON}, L_{ON} + 1, \dots, L_{Off} \quad (\text{Equation H})$$

$$latency_{OFF} = \max(s_t) | t = L_{OFF}, L_{OFF} + 1, \dots, 2 * L_{OFF} - L_{ON} \quad (\text{Equation I})$$

Results

Consistent with previous findings, the *wt* adult shows significantly more dominance of responses as seen in **Figure 10**. This supports previous findings that *wt* adult retinal ganglion cells having segregated into more ON or OFF roles (Tian et al, 2003). The *wt* P14 and *rdl* P14 exhibit more responses to both onset and offset of stimuli indicating a lower RDI and a larger number of ON/OFF cells. No significant difference was observed in the Response Dominance Index between *wt* P14 and *rdl* P14 (Kruskal-Wallis, $p = 0.43$; Daniel, 2005).

In *wt* almost all responses showed a latency of less than 160 milliseconds. By contrast, in *rdl*, a significantly delayed response occurs (**Figure 11**). Additionally, the *rdl* P14 group shows responses to low luminance stimuli are less transient than those to bright stimuli (**Figure 12**). The *wt* P14 cells show an increase in transientness with low to mid light intensity and a decrease in transientness with bright stimuli. These data are

consistent with the increased latency of the *rdl* cells in **Figure 11**. However, and increased latency does not necessarily imply suppression of responses, thus complicating the interpretation of the data.

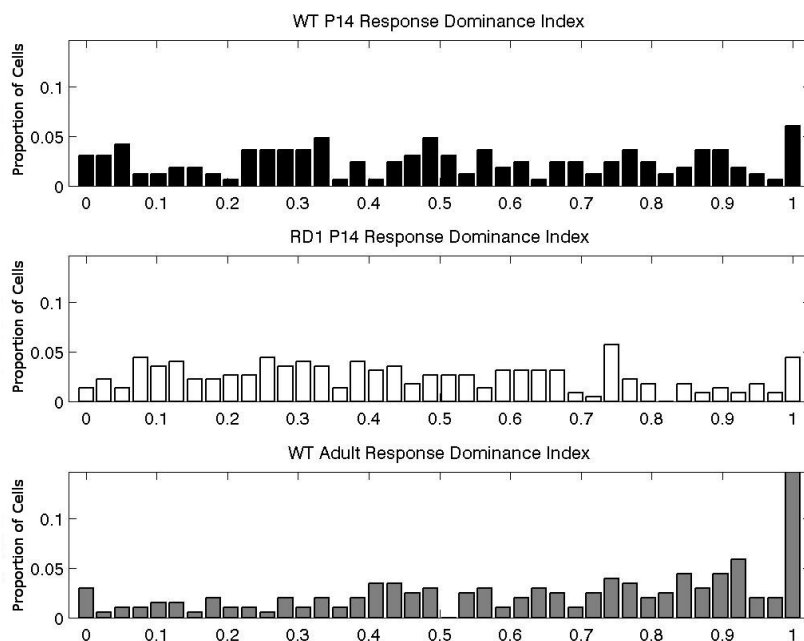


Figure 10. Response Dominance Indices. The *wt* adult shows significantly more dominance of responses as indicated by the large peak at Index = 1 using **Equation E** ($p < 10^{-7}$, Kruskal-Wallis; Daniel, 2005).

No significant changes in latency to offset of light were observed (**Figure 13**).

Three apparent groups were observed in both *wt* and *rdl*. The peak at the lowest timebin represents cells whose peak response occurred quickly after light offset, possibly indicative of ON sustained cells whose response carries into the OFF period. The middle group represents cells responding briskly. The third, smaller group at greater time values indicate a subset of delayed OFF responses.

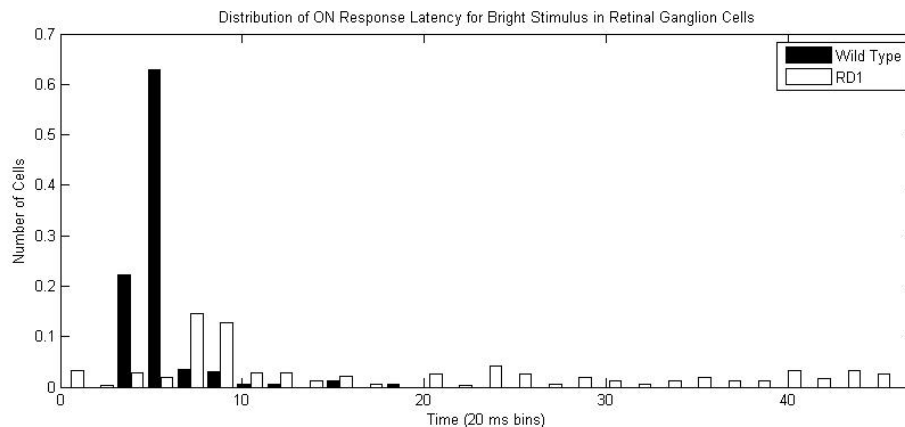


Figure 11. Latency of ON Responses at Brightest Stimulus. Using Equation G, the *rd1* P14 group shows a significantly longer latency compared to the *wt* P14 ($p < 10^{-12}$, Kruskal-Wallis; Daniel, 2005).

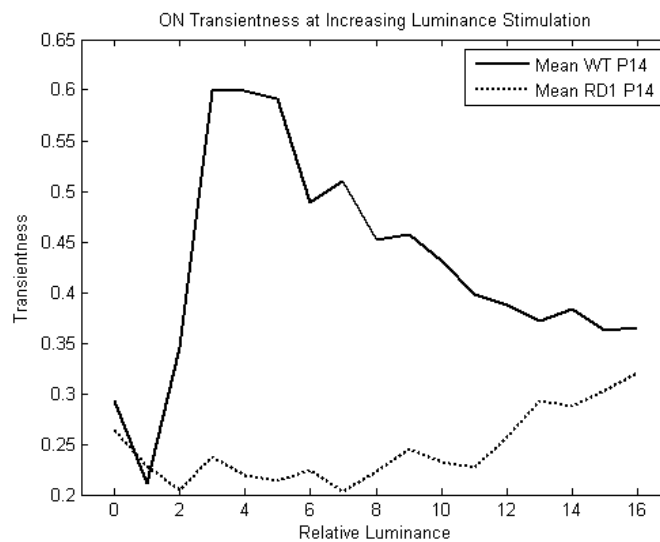


Figure 12. Transientness of Cellular Responses at Each Stimulus Intensity. Using Equation F, the *rd1* P14 group shows increasing transientness with brighter stimuli. The *wt* P14 cells have transient responses with low to mid light intensity stimuli and responses become more sustained as stimulus intensity increase.

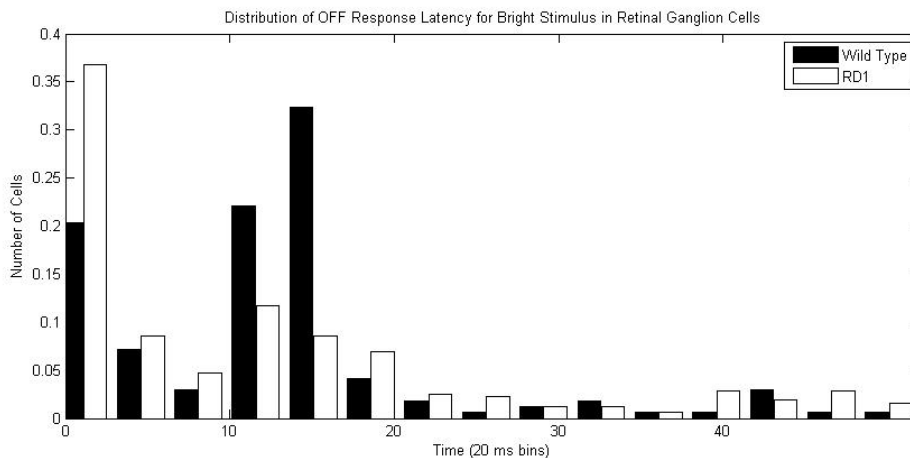


Figure 13. Off Latencies at Brightest Stimulus. Using **Equation C**, no significant change in latency from offset of light was observed ($p=0.26$, Kruskal-Wallis; Daniel, 2005).

Discussion

Maturation of visual pathways depends on both light evoked activity and on molecular mechanisms that are not activity-dependent. The separation of light and dark signals along visual processing pathways aids in contrast detection, underscoring the important for developmental segregation into ON and OFF pathways. Early in retinal development, diffuse stratification occurs in the inner plexiform layer, giving rise to a majority of retinal ganglion cells that respond to both the onset and offset of a light stimulus. Adult *wt* retinas exhibit fewer retinal ganglion cells responding to both light onset and offset, instead showing more ON or OFF cells than ON/OFF cells, as seen in **Figure 10**. In the immature *wt* retina, a subset of ON/OFF cells exist that will subsequently mature into ON cells, and another subset of ON/OFF cells mature into OFF cells: the rest will retain their response properties.

The divergence of a retinal ganglion cell's response characteristics is primarily due to "pruning" of ganglion cell dendrites in the inner plexiform layer, where bipolar

cells synapse with retinal ganglion cells. This pruning is largely activity dependent, and profoundly influences the signaling properties of the retina (Xia et al, 2007). Dark-rearing or blocking glutamate transmission in the developing retina disrupts dendritic stratification (Tian et al, 2003). Proper signaling of visual information from the photoreceptors to the ganglion cells and beyond is essential for optimally decoding images. Whether or not this pruning is driven by optimization of information transfer within the inner plexiform layer remains to be elucidated; nevertheless, some type of controlled activity is required for proper stratification.

A subset of OFF-BCs have been shown to use the amacrine cell network to effectively high pass filter responses in the ON pathway (Molnar et al, 2007). Such filtering might normally act to modulate contrast adaptation (Puopolo et al, 2001; Witkovsky, 2004; Siminoff, 1985). In the healthy retina, suppression of weak responses in the ON pathway occurs through this mechanism if the OFF pathway is more strongly stimulated than the ON pathway. Given my proposal that the OFF pathway is up-regulated in *rd1* mice, one might expect that weak ON signals would be still further suppressed in *rd1* than in *wt* mice, not only during acute and transient OFF responses, but continuously during baseline activities. Such suppression of weak ON signals is evident in the increased latency period in response to stimulus (**Figure 11**), and the decreased transientness of the *rd1* at low light stimulation (**Figure 12**). The increased latency could be the result of amacrine cells high pass filtering the ON bipolar cells. I propose that as a result of the increased glutamate concentration in the OPL and consequent up-regulation of the OFF pathway, the ON pathway is further suppressed in *rd1*.

The aforementioned mechanisms may also explain the decreased spike count observed at high luminance levels (**Figure 5**) in degeneration. The most obvious change is the reduced number of photoreceptors in *rd1* at postnatal day 14. As a majority of the outer segments have been lost by this age, the inner segments would be much less efficient at generating visual signals (Farber et al, 1994). Gain mechanisms in the inner nuclear layer could in theory compensate for this reduced response to light. Consistent with this, the b-wave amplitude of the electroretinogram peaks at this age in *rd1* (Sernagor et al, 2001). This indicates that the cones are able to relay ON signals using the intact inner circuitry of the retina. However, the responses are still reduced when compared to the *wild type*. The inhibition from the OFF pathway likely manifests itself even at the brightest stimulus. I propose that a decrease in photoreceptor number and the filtering effects of the up-regulated OFF pathway contribute to reduced spike output of the *rd1* cells in response to bright stimuli and an increase in spontaneous activity. Revisiting **Figure 9**, the shift marked as (3) would be a result of this filtering effect. These differences in the retina are illustrated in **Figure 14**.

Preservation of the OFF response beyond postnatal day 14 in *rd1* mice indicates light detection occurs well after the loss of rods (Stasheff, 2008). Such responses also indicate that components within the OFF pathway are still intact. The results in **Figure 13** support this claim, showing no temporal changes in OFF responses. High levels of glutamate could sustain the iGluRs, causing proportionately smaller fluctuations in glutamate concentration to have little effect on the number of bound receptors. The presence of OFF responses at this age supports the proposed up-regulation of the OFF pathway.

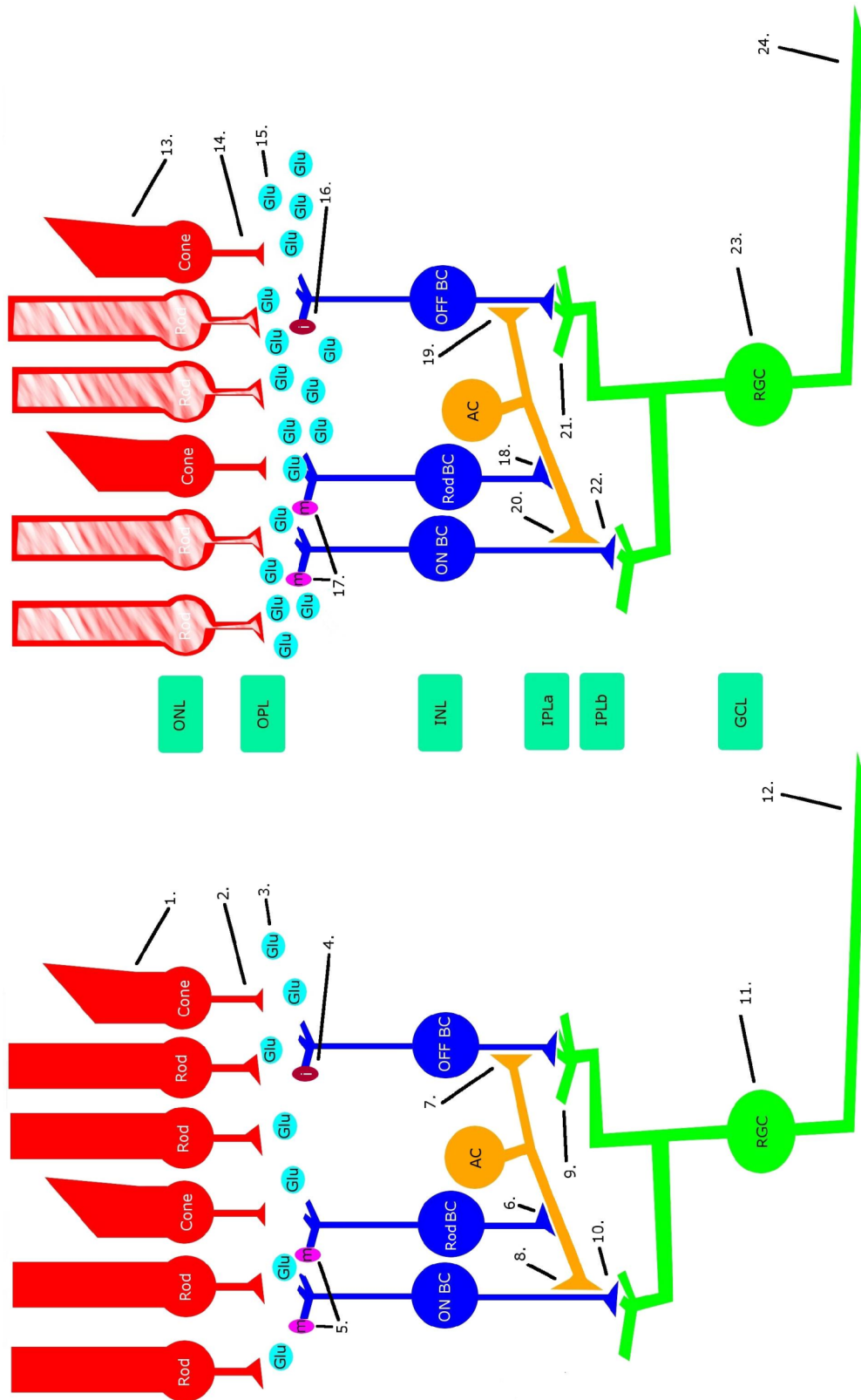


Figure 14. Proposed Model of *wt* Retina (left) Compared to *rd/rd* Retina (right). By P14, rods in *rd/rd* are rapidly

Figure 14—continued degenerating, though cones are still intact. (13) Light is absorbed in the residual photoreceptors, causing hyperpolarization of the cell. (14) Upon hyperpolarization, glutamate release from the cone pedicles decreases. (15) Because baseline glutamate concentration within the OPL is increased as compared to *wt* (3), cone activation causes proportionately less decrease in glutamate concentration in the OPL than in *wt*. (16) Ionotropic receptor activation is up-regulated compared to *wt* (4) by the increased glutamate concentration in the OPL. These receptors deactivate when glutamate concentration falls. (17) The decrease in glutamate concentration decreases the ongoing activation of the metabotropic glutamate receptors, which decreases the hyperpolarization by G-protein signaling. Due to the increased baseline concentration of glutamate in the OPL, proportionately less mGluR inactivation may occur, reducing strength of ON signaling (18,22). (19) Up-regulation of the OFF-BC increases the amacrine cell high pass filter strength, more strongly suppressing signals in the ON-BCs (20). As OFF-BCs are deactivated with light onset, the amacrine cell mediated suppression decreases. (21) Up-regulation of the OFF-BCs causes increased glutamate release in IPLa, leading to an increase in RGC spontaneous activity. (22) ON-BCs synapse with RGCs in IPLb, but due to the decrease in photoreceptor density and up-regulation of ON-inhibition compared to *wt* (10), the ON-BCs transmit significantly weaker signals to the RGCs. Retinal ganglion cells integrate signals from both OFF and ON pathways within the dendrites (21, 22) and soma (23), as is also the case in *wt* (9,10,11). Spikes are generated at the initial segments in the RGCs and transmitted via the axons to the brain (24). Abbreviations: Am, amacrine cell; Glu, glutamate; i, ionotropic glutamate receptor; INL, inner nuclear layer; IPLa, inner plexiform layer sublamina *a*; IPLb, inner plexiform layer sublamina *b*; m, metabotropic glutamate receptor; OFF-BC, off bipolar cell; ON-BC, on bipolar cell; ONL, outer nuclear layer; PhR, photoreceptor; RGC, retinal ganglion cell. Note: horizontal and Muller cells have been omitted for clarity.

If noise is suppressed in ON pathway signaling, full useful vision can not be generated in disease by simply adding light to visual scenes. Note that useful vision involves contrasting images. Contrast is a difference in luminance between adjacent objects, which invariably must involve the OFF pathway. Any useful vision-forming stimulus would thus contain OFF pathway carried by the noise. This illustrates a potential advantage for using full field stimuli: noise from the OFF pathway may be optimally reduced. Since images with contrast inherently contain regions darker than others, OFF pathway noise may permeate any transmitted message from the retinal

ganglion cells. Moreover, stimuli such as white noise or m-sequence would also cue OFF signaling.

In the following chapter, I present a set of computational methods to further explain the response characteristics of retinal ganglion cells in degeneration.

Future Studies

The mechanisms proposed in this chapter could be tested by single cell recordings of amacrine cell function in retinal degeneration. One could study the paired relations between amacrine cells and OFF bipolar cells, and the effect of noise on inhibition of ON signaling. More complex stimuli, such as white noise, gratings, real world images, or m-sequences, could be used to elucidate how parallel pathways are disrupted in degeneration.

CHAPTER VI: INFORMATION CAPACITY IN DEGENERATION

In this chapter, I present a useful set of tools that help explain and corroborate the findings in the previous chapters. I use information theoretic methods to quantify the ability of retinal ganglion cells to transmit useful messages to the brain. It is my goal to show that information theoretic methods are useful in understanding disease, and that the results of utilizing these methods support the observations and hypotheses in the previous chapters.

Computational Methods

Estimates of naive entropy were calculated by allocating all spikes into 20 millisecond timebins, creating "words" for each cluster of spikes. In order to find the group's naive entropy, or the entropy of the spike train regardless of stimuli, all probabilities of observing each word multiplied by the logarithm of each probability are summed (**Equation J**) (Shannon, 1948),

$$Entropy_{naive} = -1 * \sum_{t=1}^{t_{max}} p_i * \log p_i \quad (\text{Equation J})$$

where p_i is the probability of observing a spike in a given time bin, and t_{max} is the maximum timebin. The sum of all probabilities is conventionally multiplied by a negative one in order to display a positive entropy value (Rieke et al, 1998).

The noise entropy was calculated by performing the same analysis in **Equation J** over non-refractory, non-stimulated periods. Each group's estimate of mutual

information between stimuli and responses was calculated by subtracting the noise entropy from the naive estimate, using the Kullback-Leibler divergence (**Equation K**) (Haykin, 1999; Rieke et al, 1997; Szallasi et al, 2006; Linsker, 1988),

$$M(S;L) = H(L) - H(L|S) = \sum_S \sum_L P(s)P(l|s) \log\left(\frac{P(l|s)}{P(l)}\right) \quad (\text{Equation K})$$

where $P(s)$ is the spike probability, $P(l)$ is the probability of the occurrence of a stimulus, and $P(l|s)$ is the probability of a stimulus occurring with a spike. These entropic values were calculated for both individual cells and whole populations, giving $M(S;L)$, the mutual information between stimulus and response, $H(L)$, the noise entropy, and $H(L|S)$ the naive entropy (Rieke et al, 1997; Strong et al, 1998).

Results

The naïve entropy estimate illustrates the overall channel capacity for message transmission. These estimates for *wt* and *rdl* retinal ganglion cells did not differ (**Figure 15**). These findings suggest that populations of retinal ganglion cells in *rdl* are still capable of signaling the same amount of information as in *wt*.

The *rdl* P14 cells show an increase in the entropy of noise (**Figure 16**), calculated as the minimum entropy among all responses at any stimulus intensity (including $I_L = 0$). This increase in noise entropy is likely due to the increase in spontaneous firing activity of retinal ganglion cells in degeneration.

Rdl retinal ganglion cells exhibited a significant decrease in the mutual information between stimuli and responses compared to *wt* P14, an indicator of reduced information transmission capacity (**Figure 17**).

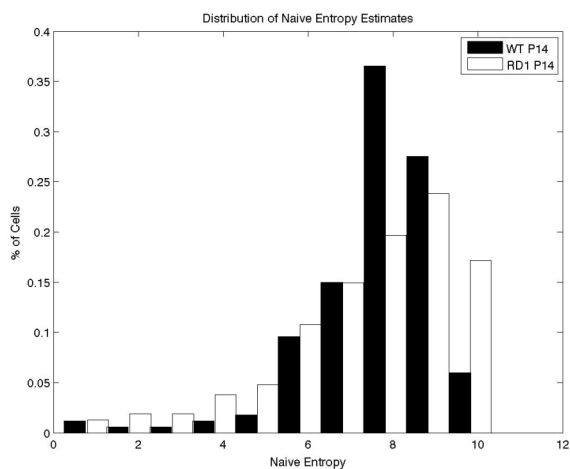


Figure 15. Naive Entropy Estimates. Using Equation J, *wt* and *rdl* retinal ganglion cells show similar aggregate estimates of naive entropy ($p = 0.93$; Daniel, 2005).

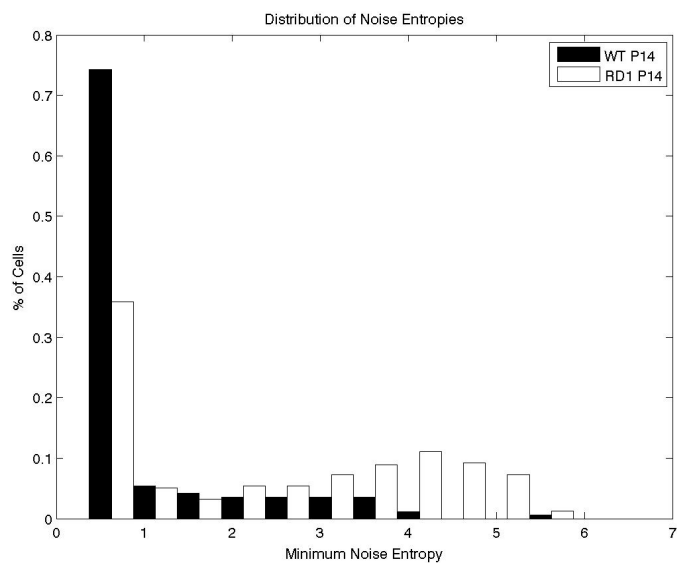


Figure 16. Entropy of Noise. Using Equation I, the *rdl* P14 cells show an increase in the entropy of noise.

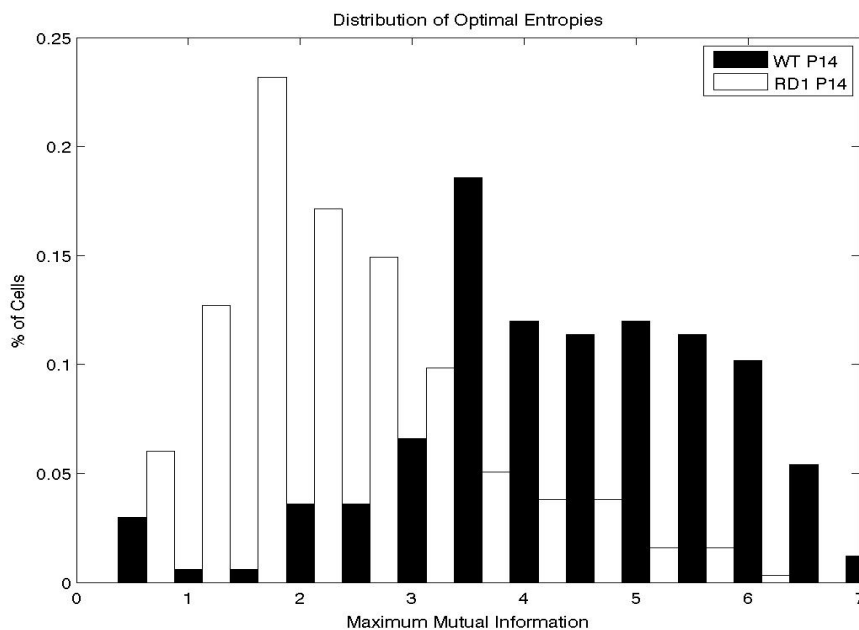


Figure 17. Mutual Information Between Stimuli and Responses. Using **Equation K**, the distribution of *rdl* P14 cells shows a significant decrease in the mutual information between stimulus and response compared to *wt* P14 (Kruskal-Wallis, $p < 10^{-10}$; Daniel, 2005).

Discussion

Information theory has shown itself to be a useful means of quantifying information capacity in communication systems (Shannon, 1948). Within the framework of information theory, Shannon entropy describes the uncertainty in messages. Used as a performance measurement for information transfer, entropic measures can show how well neurons transmit useful information (Rieke et al, 1998). Shannon entropy is the probability of a message's occurrence given equal probability of all possible messages.

The identification of useful information involves subtracting the “bad information” from the total information (Deco et al, 1998). Bad information is commonly referred to as the *noise entropy*. As in Webster's second definition, noise

entropy causes a corruption of the desired message. Optimal neural systems are able to relay useful output given useful input, and likewise relay no output if the input is of no utility¹. One of the retina's functions is to optimize contrast in visual scenes before relaying a message (Prokopowicz et al, 1995). If the contrast optimization is disrupted, many of the retina's unique capabilities are hindered (Passaglia et al, 2004). Downstream neurons cannot fulfill their duties if they are given bad information. Performance of information transfer is thus crucial in neural systems.

One practical method of group entropy estimation used in speech and pattern recognition is the Kullback-Leibler (KL) divergence (Filippone et al, 2010). The KL divergence is a statistical tool for estimating the probability of difference in information between two systems (Hershey et al, 2007). In Bayesian statistics, it is used for estimating the maximum distance between a prior distribution and a posterior distribution (Goutis et al, 1998). Applied here, the KL divergence is used to estimate the distribution of information in one state and compare this with the distribution of information in another state. Since a primary goal here is to separate good information from bad

¹ E.g., take a given spike train, one spike every one second, without perturbation. Fixing the start time, the message can be described in only one possible manner over any period of time: one spike occurs, like clockwork, every second. One could be very certain of the spike arrival times here. The rate of information transmission for any time period is fixed and can be easily calculated: one bit per second. A high fidelity downstream neuron could relay each spike by transmitting one spike in each instance. In this case information would be conserved. This downstream neuron could expend much more energy and transmit, say, 1000 spikes over the span of one second in response to the single spike input. If **Equation J** is used, and each spike is binned individually, the apparent information rate in this secondary neuron jumps to 6.91 bits/s. Such a high bit count occurs because there are a large number of ways 1000 spikes can be arranged within the allocated time period. It remains uncertain when these 1000 spikes will occur without any *a priori* knowledge. Thus, the uncertainty in the system is high, and the entropy is correspondingly high. But clearly the upstream neuron has not packaged any additional information into its single spike per second. This does not necessarily imply the downstream neuron is giving false information, only that it transmits the information it receives in a less certain and less efficient manner. The downstream neuron places an upper bound on the information transfer characteristics of the system. Finding this upper bound is of no use if the entropy of the noise and the input bias are not taken into account.

information, the maximum distance between distributions of information in all states of response is calculated (**Equation K**). In finding this maximum distance, no assumptions need to be made with regards to what are optimal stimuli for a given cell. Since cells exhibit a wide range of response characteristics to different stimuli, the maximal difference in entropy between any two stimulus states is the maximum amount of unique information a given cell can transmit within the range of stimulus parameters chosen (Linsker, 1988).

Differences in the information carrying capacity among different cell populations in the visual system may be used to quantify how vision is altered in disease. Once having estimated a maximum information rate of 400,000 bits/s in the normal mouse retina (Koch et al, 2004), reductions in individual and population entropies may be used to show how much less information is transmitted in disease states. Such an upper bound on population estimates in the normal retina has one major limitation. Without any attempt to identify correlation or redundancy of information among the cells of the population, the realized information input to the cortex will be less than estimated (Brody, 1999; Schneidman et al, 2003). Correlation in neural networks is thought to be a property that conveys emphasis (Averbeck et al, 2006). Energy consumption often pays the price in correlation coding, suggesting a bias toward metabolically efficient spike codes (Balasubramanian et al, 2002). Given these constraints, it is assumed that in the presence of correlation, useful information drops below the upper bound set by estimated Shannon entropy. Adaptive compensation mechanisms by downstream neurons in the dLGN or cortex in disease are also not considered. Image perception in disease might be

enhanced by compensatory cortical function, though such a possibility is beyond the scope of this discussion.

Despite functional changes, increased spontaneous activity and a decreased maximal response do not preclude retinal ganglion cells in *rdl* from transmitting useful information. **Figure 15** shows that *rdl* retinal ganglion cells have the capacity to transmit information. Even though the mutual information between stimulus and response is reduced, as seen in **Figure 17**, one could speculate that a broad dynamic range in the responses of RGCs might be able to compensate for the presence of noise and reduced mutual information. However, the distribution of slopes at each cell's I_{50} shows that *rdl* cells include a larger subset of cells with restricted dynamic range. These cells have nearly an *all or none* effect in information transfer. The restricted dynamic range is evident in the increased slope observed in the response profiles of the *rdl* cells. The increased spontaneous activity and nonlinear effects of such “noise” may contribute to the reduced dynamic range and information capacity of *rdl* retinal ganglion cells compared to *wt*.

If spontaneous firing is a result of OFF pathway up-regulation, then under continuous stimulation with bright light, noise should be suppressed in the OFF pathway. One cannot be entirely certain that this is the case in *rdl*.

How the brain perceives spiking noise is another concern. No *a priori* knowledge is provided to the downstream neurons regarding stimulus conditions. A burst of spontaneous activity could appear identical to a burst in response to light stimulation. Without any other information, a perceptual network cannot discriminate between such

messages. It is thus crucial to understand the difference between the two conditions that yields the maximum mutual information between an optimal stimulus and its response.

Future Studies

The methods discussed in this chapter could be applied to the studies proposed at the end of Chapter V. One could deduce what the brain “sees” in degeneration using “natural” stimuli and implementation of a computational model that accounts for the observed functional changes. Many current strategies to rescue vision, including electronic stimulation and gene therapy, heavily rely on a functional inner retina (Kelly et al, 2009). The data presented here suggest that capacity for information transfer is reduced but still substantial early in disease. Retinal prosthesis research groups can benefit by understanding the communication limits of target cells. Much can be learned by understanding mechanisms of inner retina malfunction in disease. For example, pharmacological intervention could target the described pathways in order to reduce the harmful effects of cell death or glutamate toxicity in early degeneration.

CHAPTER VII: CONCLUSION

In this thesis, I demonstrate the utility of a range of quantitative techniques, including communication theory, and apply these to electrophysiologic recordings to characterize functional changes that occur in early stages of retinal degeneration in the mouse. I use these techniques to show novel findings. Early in disease, retinal ganglion cells in the *rd1* mouse exhibit interesting differences from their *wild type* counterparts. An increased latency of responses to the onset of a light stimulus, decreased spike count in response to stimulus onset, increased spontaneous firing activity, and a decrease in information transmission are observed in this animal model of inherited retinal degeneration. Some potential future studies are proposed that might offer a means of further elucidating the impact of this blinding eye disease. The use of innovative techniques provides a framework for proposing that up-regulation of OFF bipolar cell excitation may be a principle mechanism responsible for the observed functional changes in the *rd1* mouse.

REFERENCES

- Alon U, An Introduction to Systems Biology. Chapman & Hall/CRC, Boca Raton, FL, 2007.
- Applebury ML, Antoch MP, Baxter LC, Chun LL, Falk JD, Farhangfar F, Kage K, Krzystolik MG, Lyass LA, Robbins JT. The murine cone photoreceptor: a single cone type expresses both S and M opsins with retinal spatial patterning. *Neuron*, 2000, 27(3):513-23.
- Arshavsky VY, Trevor D. Lamb, and Edward N. Pugh, Jr. G Proteins and Phototransduction. *Annual Review of Physiology*, 2002, 64: 153-187.
- Averbeck BB, Latham PE, Pouget A. Neural correlations, population coding and computation. *Nature Reviews*, 2006, 7: 358-366.
- Badea TC, Nathans J. Quantitative analysis of neuronal morphologies in the mouse retina visualized by using a genetically directed reporter. *J Comp Neuro*, 2004, 480:331-351.
- Balasubramanian V, Kimber D, Berry MJ. Metabolically Efficient Information Processing. *Neural Comp*. MS 2132.
- Balkema GW Jr, Pinto LH. Electrophysiology of retinal ganglion cells in the mouse: a study of a normally pigmented mouse and a congenic hypopigmentation mutant, pearl. *J Neurophysiol*, 1982, 48: 968-979.
- Baylor DA, T D Lamb, and K W Yau. The membrane current of single rod outer segments, *J Physiol*, 1979, 288: 589-611.
- Berciano J, Lafarga M. Santiago Ramon y Cajal (1852-1934). *J Neurol*, 2001, 248(2):152-153.
- Bisti S, Cargini C, Chalupa LM. Blockade of Glutamate-Mediated Activity in the Developing Retina Perturbs the Functional Segregation of ON and OFF Pathways. *J Neurosci*, 1998, 18(13):5019-5025.
- Blanks JC, Adinolfi AM, Lolley RN. Photoreceptor degeneration and synaptogenesis in retinal-degenerative (rd) mice. *J Comp Neurol*, 1974, 156:95-106.
- Bowes C, Li T, Danciger M, Baxter LC, Applebury ML, Farber DB. Retinal degeneration in the rd mouse is caused by a defect in the B subunit of rod cGMP-phosphodiesterase. *Nature*, 1990, 437:677-680.
- Brody CD. Correlations without synchrony. *Neural Computation*, 1999, 11:1537-1551.
- Carroll SM. From Eternity to Here: The Quest for the Ultimate Theory of Time. Dutton, 2010.
- Casti A, Hayot F, Xiao Y, Kaplan E. A simple model of retina-LGN transmission. *J Comput Neurosci*, 2008, 24(2):235-52.
- Chan TL, Martin PR, Clunas N, Grunert U. Bipolar Cell Diversity in the Primate Retina: Morphologic and Immunocytochemical Analysis of a New World Monkey, the Marmoset *Callithrix jacchus*. *J Comp Neurol*, 2001, 437:219-239.

- Clark BA, Cull-Candy SG. Activity-Dependent Recruitment of Extrasynaptic NMDA Receptor Activation at an AMPA Receptor-Only Synapse. *J Neurosci*, 2002, 22(11):4428-4436.
- Daniel WW, Biostatistics: A Foundation for Analysis in the Health Sciences. Wiley, 2005.
- Dayan P and Abbott LF, Theoretical Neuroscience: Computational and Mathematical Modeling of Neural Systems, MIT Press, Cambridge, MA, 2001.
- Deco G, Schurmann B. Stochastic resonance in the mutual information between input and output spike trains of noisy central neurons. *Physica D*, 1998, 117:276-282.
- Delyfer MN, Forster V, Neveux N, Picaud S, Leveillard T, Sahel JA. Evidence for glutamate-mediated excitotoxic mechanisms during photoreceptor degeneration in the *rd1* mouse retina. *Molecular Vision*, 2005, 11:688-96.
- Diao L, Wenzhi Sun, Qiudong Deng, Shigang He. Development of the mouse retina: Emerging morphological diversity of the ganglion cells. *Journal of Neurobiology*. 61(2):236-249.
- Famiglietti EV Jr, Kolb H. Structural basis for ON-and OFF-center responses in retinal ganglion cells. *Science*, 1976, 194(4261):193-195.
- Farber DB, Flannery JG, Bowes-Rickman C. The *rd* mouse story: Seventy years of research on an animal model of inherited retinal degeneration. *Prog Ret Eye Res*, 1994, 13(1):31-64.
- Filippone M, Sanguinetti G. Information theoretic novelty detection. *Pattern Recognition*, 2010, 43:805-814.
- Firth SI, Wang CT, Feller MB. Retinal waves: mechanisms and function in visual system development. *Cell Calcium*, 2005, 37(5):425-432.
- Foster RG. Keeping an Eye on the Time: The Cogan Lecture. *IOVS*, 2002, 43(5):1286-1298.
- Fu Y, Yau KW, Phototransduction in mouse rods and cones. *Eur J Physiol*, 2007, 454:805-819.
- Hackam AS, Strom R, Liu D, Qian J, Wang C, Otteson D, Gunatilaka T, Farkas RH, Chowes I, Kageyama M, Leveillard T, Sahel JA, Campochiaro PA, Parmigiani G, Zack DJ. Identification of gene expression changes associated with the progression of retinal degeneration in the *rd1* mouse. *Invest Ophthalmol Vis Sci*, 2004, 45(9):2929-2942
- Han Y, Massey SC. Electrical synapses in retinal ON cone bipolar cells: subtype-specific expression of connexins. *PNAS*, 2005, 102(37):13313-13318.
- Harveit E. Functional organization of cone bipolar cells in the rat retina. *J Neurophysiol*, 1997, 77(4):1716-1730.
- Haykin S. Neural Networks: A Comprehensive Foundation, 2nd Edition. Prentice Hall, NJ, 1999.

- Helmholz H. *Handbuch der Physiologischen Optik*, 1867. Accessed via the Internet on 28 Feb, 2010.
[http://books.google.com/books?id=E3EZA AAA YAAJ&pg=PA877&lpg=PA877&dq=Handbuch+der+Physiologischen+Optik&source=bl&ots=ynGhizf8Cy&sig=B9Uuo-hT_MpfLdud6VUtuRefYCc&hl=en&ei=ZaeKS_b-CIa6No3f8KUB&sa=X&oi=book_result&ct=result&resnum=5&ved=0CBwQ6AEwBA#v=onepage&q=&f=false]
- Hershey J, Olsen P. Approximating the Kullback Leibler divergence between Gaussian mixture models. *Proc ICASSP*, 2007, 317-320.
- Hubel DH, Wiesel TN. Receptive fields of single neurones in the cat's striate cortex. *J Physiol*, 1959, 148:574-91.
- Humayun MS, Weiland JD, Chader G, Greenbaum E (eds). Artificial Sight: Basic Research, Biomedical Engineering, and Clinical Advances. Springer, New York, NY, 2007.
- Izhikevich EM. Dynamical Systems in Neuroscience: The Geometry of Excitability and Bursting. MIT Press, 2007.
- Jeon CJ, Strettoi E, Masland RH. The Major Cell Populations of the Mouse Retina. *J Neurosci*, 1998, 18(21):8936–8946.
- Keeler, CE. The inheritance of a retinal abnormality in white mice. *PNAS*, 1924, 10:329-333.
- Kelly SK, Shire DB, Chen J, Doyle P, Gingerich MD, Drohan WA, Theogarajan LS, Cogan SF, Wyatt JL, Rizzo JF. Realization of a 15-channel, hermetically-encased wireless subretinal prosthesis for the blind. *Conf Proc IEEE Eng Med Biol Soc*. 2009; 2009:200-3.
- Koch K, McLean J, Segev R, Freed MA, Berry MJ, Balasubramanian V, Sterling P. How Much the Eye Tells the Brain. *Current Biology*, 2006, 16(14):1428-1434.
- Lambda D, Nelson B, Karl MO, Reh TA. In Eye, Retina, and Visual System of the Mouse. Chalupa LM, Williams RW (eds). MIT Press, 2008, pp 299-310.
- LaVail MM, Matthes MT, Yasumura D, Steinberg RH. Variability in rate of cone degeneration in the retinal degeneration (rd/rd) mouse. *Exp Eye Res*, 1997, 65:45-50.
- Linsker R. Self-organization in a perceptual network. *TC*, 1988, 105-117.
- Lucas DR, Newhouse JP. The Toxic Effect of Sodium L-Glutamate on the Inner Layers of the Retina. *Arch Ophth*, 1957, 58(2):193-201.
- Marc RE. Mapping glutamatergic drive in the vertebrate retina with a channel-permeant organic cation. *J Comp Neurol*, 1999, 407:47-64.
- Marc RE, Jones BW, Watt CB, Strettoi E. Neural remodeling in retinal degeneration. *Prog Ret Eye Res*, 2003, 22:607-655.
- Margaret A. MacNeil and Richard H. Masland. Extreme Diversity among Amacrine Cells: Implications for Function. *Neuron*, 1998, 20:971–982.

- Masland RH. Maturation of function in the developing rabbit retina. *J Comp Neurol*, 1977, 175(3):253-371.
- Masland RH. The fundamental plan of the retina. *Nature Neuroscience*, 2001, 4:877-886.
- Meister M, Pine J, Baylor DA. Multi-neuronal signals from the retina: acquisition and analysis. *J Neurosci Methods*, 1994, 51: 95–106.
- Molnar A, Werblin F. Inhibitory feedback shapes bipolar cell responses in the rabbit retina. *J Neurophys*, 2007, 98:3423-3435.
- Mu X, Klein WH, In Eye, Retina, and Visual System of the Mouse. Chalupa LM, Williams RW (eds). MIT Press, 2008, pp 321-332.
- Münch TA, da Silveira RA, Siegert S, Viney TJ, Awatramani GB, Roska B. Approach sensitivity in the retina processed by a multifunctional neural circuit. *Nature Neuroscience*, 2009, 12, 1308-1316.
- “Noise.” Webster’s Third New International Unabridged Dictionary. Merriam-Webster. 2002.
- Olney JW. Glutamate-Induced Retinal Degeneration in Neonatal Mice. Electron Microscopy of the Acutely Evolving Lesion. *J Neuropath Exp Neurol*, 1969, 28(3):455-474.
- Pan F, Paul DL, Bloomfield SA, Völgyi B. Connexin36 is required for gap junctional coupling of most ganglion cell subtypes in the mouse retina. *J Comp Neurol*. 2010, 518(6):911-927.
- Passaglia CL, Troy JB. Information transmission rates of cat retinal ganglion cells. *J Neurophysiol*, 2004, 91:1217-1229.
- Passaglia CL, Troy JB. Impact of noise on retinal coding of visual signals. *J Neurophysiol*, 2004, 92:1023-1033.
- Phelan JK, Bok D. A brief review of retinitis pigmentosa and the identified retinitis pigmentosa genes. *Molecular Vision*, 2000, 6:116-124.
- Portera-Cailliau C, Sung CH, Nathans J, Adler R. Apoptotic photoreceptor cell death in mouse models of retinitis pigmentosa. *Proc Natl Acad Sci*, 1994, 91:974-978.
- Prokopowicz PN, Cooper PR. The dynamic retina: Contrast and motion detection for active vision. *Int J Comp Vis*, 1995, 16(3):191-204.
- Puopolo M, Hochstetler SE, Gustincich S, Wightman RM. Extrasynaptic release of dopamine in a retinal neuron: Activity dependence and transmitter modulation. *Neuron*, 2001, 30:211-225.
- Rieke F, Warland D, van Stevenick RR, Bialek W. Spikes: Exploring the Neural Code. MIT Press, 1997.
- Rousseau D, Varela JR, Chapeau-Blondeau F. Stochastic resonance for nonlinear sensors with saturation. *Physical Review E*, 2003, Epub, 67(2), 021102.
- Ruddel BL, Kumar P. Ecohydrological Process Networks: 1. Identification. *Water Resources Research*, 2009, 45, Epub, W03419.

- Sancho-Pelluz J, Arango-Gonzalez B, Kustermann S, Romero FJ, van Veen T, Zrenner E, Ekstrom P, Paquet-Durand F. Photoreceptor Cell Death Mechanisms in Inherited Retinal Degeneration. *Mol Neurobiol*, 2008. 38:253-269.
- Schmidt TM, Kofuhi P. Functional and Morphological Differences among Intrinsically Photosensitive Retinal Ganglion Cells. *J Neurosci*, 2009, 29(2):476-482.
- Schmidt JT, Eisele LE. Stroboscopic illumination and dark rearing block the sharpening of the regenerated retinotectal map in goldfish. *Neuroscience*, 1985, 14(2):535-546.
- Schneidman E, Bialek W, Berry MJ. Synergy, redundancy, and independence in population codes. *J Neurosci*, 2003, 23(37):11539-53.
- Segev R, Goodhouse J, Puchalla J, Berry II M. Recording spikes from a large fraction of the ganglion cells in a retinal patch. *Nat Neurosci*, 2004, 7:1154-1161.
- Sernagor E, Eglen SJ, Wong ROL. Development of retinal ganglion cell structure and function. *Prog Ret Eye Res*, 2001, 20(2):139-174
- Shannon CE. A Mathematical Theory of Communication. Bell Systems Tech, 1948.
- Shatz CJ. Emergence of order in visual system development. *PNAS*, 1996, 93(2):602-608.
- Siminoff R. Dynamics of L-type bipolar and phasic amacrine cells in the vertebrate cone retina. *Biol Cybern*, 1985, 53(2):125-135.
- Stasheff SF. Emergence of sustained spontaneous hyperactivity and temporary preservation of OFF responses in ganglion cells of the retinal degeneration (rd1) mouse. *J Neurophysiol*, 2008, 99(3):1408-1421.
- Sterling P, Freed M. How robust is a neural circuit? *Visual Neuroscience*, 2007, 24:563-571.
- Stevens JK, Gerstein GL. Interactions between cat lateral geniculate neurons. *J Neurophys*, 1976, 39(2):239-256.
- Stone C, Pinto LH. Response properties of ganglion cells in the isolated mouse retina. *Vis Neurosci*, 1993, 10:31-39.
- Strettoi E, Porciatti V, Falsini B, Pignatelli V, Rossi C. Morphological and functional abnormalities in the inner retina of the rd/rd mouse. *J Neurosci*, 2002, 22(13):5492-5504.
- Strong SP, Koberle R, de Ruyter van Steveninck RR, Bialek W. Entropy and Information in Neural Spike Trains. *Physical Review Letters*. 80(1):197-200, 1998.
- Stryker MP, Harris WA. Binocular impulse blockade prevent sthe formation of ocular dominance columns in cat visual cortex. *J Neurosci*, 1986, 6(8):2117-33.
- Szallasi Z, Stelling J, Periwal V (eds). System Modeling in Cellular Biology, MIT Press, Cambridge, MA, 2006.
- Thompson S, Foster RG, Stone EM, Sheffield VC, Mrosovsky N. Classical and melanopsin photoreception in irradiance detection: negative masking of locomotor activity by light. *Eur J Neurosci*. 2008, 27(8):1973–1979.

- Thoreson WB, Babai N, Bartoletti TM, Feedback from Horizontal Cells to Rod Photoreceptors in Vertebrate Retina. *J Neurosci*, 2008, 28(22):5691-5695.
- Tian N, Copenhagen DR. Visual stimulation is required for refinement of ON and OFF pathways in postnatal retina. *Neuron*, 2003, 39:85-96.
- Tremain KE, Wong RO. Physiological deficits in the visual system of mice infected with Semliki Forest virus and their correlation with those seen in patients with demyelinating disease. *Brain*, 1983, 106: 879-895.
- Volgyi B, Deans MR, Paul DL, Bloomfield SA. Convergence and segregation of the multiple rod pathways in mammalian retina. *J Neurosci*, 2004, 24(49):11182-11192.
- Wallisch P, Lusignan M, Benayoun M, Baker TI, Dickey AS, Hatsopoulos NG. MATLAB for Neuroscientists: An Introduction to Scientific Computing in MATLAB, Academic Press, Burlington, MA, 2009.
- Wassle H, Puller C, Muller F, Haverkamp S. Cone contacts, mosaics, territories of bipolar cells in the mouse retina, *J Neurosci*, 2009, 29(1):106-117.
- Wheeler BC. Automated discrimination of single units. *Methods for Neural Ensemble Recordings*, Nicolelis MAL (ed). Boca Raton, FL: CRC, 1999, pp 61–77.
- Wilson JR, Bullier J, Norton TT. Signal-to-noise comparison for X and Y cells in the retina and lateral geniculate nucleus of the cat. *Exp Brain Res*, 1988, 70:399-405.
- Witkovsky P. Dopamine and retinal function. *Documenta Ophthalmologica*, 2004, 108:17-40.
- Wollman DE, Palmer LA. Phase locking of neuronal responses to the vertical refresh of computer display monitors in cat lateral geniculate nucleus and striate cortex. *J Neurosci Methods*, 1995, 60: 107–113.
- Wong ROL, Retinal waves and visual system development. *Annu Rev Neurosci*, 1999, 22:29-47.
- Wu SM, Yang XL. Electrical coupling between rods and cones in the tiger salamander retina, *PNAS*, 1988 85:275-278.
- Xia Y, Nawy S, Carroll RC. Activity-dependent synaptic plasticity in retinal ganglion cells. *J Neurosci*, 2007, 27(45):12221-12229.

APPENDIX: MATLAB DOCUMENTATION

```

%%%%%%%%%%%%%%%%%%%%%%%%%%%%%%%%%%%%%%%%%%%%%%%%%%%%%%%%%%%%%%%%%%%%%%%%
%
%   avgRandFF_E.m
%
%   Programmer: Erik Nylen, Stasheff Lab, University of Iowa
%   Based on software originally written by Steven Stasheff.
%   Software edited to reasonable size to fit within thesis.
%
%   Inputs:
%   N1: an 88x12 cell, each cell contains an array of
%   values indicating number of spikes contained within 20
%   millisecond timebins over entire experiment.
%
%   logdata: a structure containing stimulus trigger values
%
%   numstims: number of stimuli in trial
%
%   trials: number of trials in experiment
%
%   Outputs:
%   main: structure containing all relevant data
%
%%%%%%%%%%%%%%%%%%%%%%%%%%%%%%%%%%%%%%%%%%%%%%%%%%%%%%%%%%%%%%%%%%%%%%%%
load N1;
load logdata;
load numstims;
load trials;
% Cycle through all available channels and units
for ch = 12:87
for u = 1:5
    if ~(isempty(N1{ch,u}))
        for s = 1:numstims
            for rep = 1:trials
                if (rep == 1)
                    % Extract binned spike data for all stimulation periods
                    main.record.cellular{ch,u}.this_sumPSTH(s,:) = ...
                        N1{ch,u}(
                            (round(logdata.splicesync(logdata.stimonuse...
                                (s,rep))-5):(round(logdata.splicesync...
                                    (logdata.stimonuse(s,rep))+(stimbins+50) ),1);
                    % Extract spike time values for all stimulation periods
                    main.record.cellular{ch,u}.rasterval{s}(rep,:) = ...
                        N1{ch,u}((round(logdata.splicesync(logdata.stimonuse...
                            (s,rep))-5):(round(logdata.splicesync...
                                (logdata.stimonuse(s,rep))+150),1);
                    % Extract baseline firing rates
                    main.record.cellular{ch,u}.this_baselinePSTH(s,:) =...
                        N1{ch,u}((round(logdata.splicesync(logdata.stimonuse...
                            (s,rep))-25):round(logdata.splicesync...
                                (logdata.stimonuse(s,rep))),1);
                    % Extract spikes for ON response periods
                    main.record.cellular{ch,u}.this_ONresp(s,:) ...

```

```

        = main.record.cellular{ch,u}.this_sumPSTH...
          (s,6:(stimbins+5));
% Extract spikes for OFF response periods
main.record.cellular{ch,u}.this_OFFresp(s,:) = ...
  main.record.cellular{ch,u}.this_sumPSTH...
    (s,(stimbins+5):(stimbins*2+5));
else % if rep ~= 1
  % hold previous spike bins
  newarray = N1{ch,u}((round(logdata.splicesync...
    (logdata.stimonuse(s,rep))-5):(round...
    (logdata.splicesync(logdata.stimonuse...
    (s,rep))+stimbins+50),1);
% Perform calculations from previous loop
main.record.cellular{ch,u}.rasterval{s}(rep,:)...
  = N1{ch,u}((round(logdata.splicesync...
    (logdata.stimonuse(s,rep))-50):(round...
    (logdata.splicesync(logdata.stimonuse...
    (s,rep))+150),1);
main.record.cellular{ch,u}.this_sumPSTH(s,:) =...
  main.record.cellular{ch,u}.this_sumPSTH(s,:)+newarray';
newbase = N1{ch,u}((round(logdata.splicesync...
  (logdata.stimonuse(s,rep))-25):round...
  (logdata.splicesync(logdata.stimonuse(s,rep))),1);
main.record.cellular{ch,u}.this_baselinePSTH(s,:) = ...
  main.record.cellular{ch,u}.this_baselinePSTH(s,:)+...
  newbase';
main.record.cellular{ch,u}.this_ONresp(s,:) = ...
  main.record.cellular{ch,u}.this_sumPSTH...
    (s,6:(stimbins+5));
main.record.cellular{ch,u}.this_OFFresp(s,:) = ...
  main.record.cellular{ch,u}.this_sumPSTH...
    (s,(stimbins+5):(stimbins*2+5));
end % end if rep == 1
end % end for rep = 1:trials
% Calculate total baselinerate
main.record.cellular{ch,u}.this_baselinerate(s) = ...

(sum(main.record.cellular{ch,u}.this_baselinePSTH(s,:)));
% Calculate total ON response for each stimulus
main.record.cellular{ch,u}.sumONresp(s) = ...
  (sum(main.record.cellular{ch,u}.this_ONresp(s,:)));
% Calculate total OFF response for each stimulus
main.record.cellular{ch,u}.sumOFFresp(s) = ...
  (sum(main.record.cellular{ch,u}.this_OFFresp(s,:)));
% Calculate net ON response
main.record.cellular{ch,u}.netONresp(s) = ...
  (sum(main.record.cellular{ch,u}.this_ONresp(s,:)) -...
  main.record.cellular{ch,u}.this_baselinerate(s));
% Calculate net OFF response
main.record.cellular{ch,u}.netOFFresp(s) = ...
  (sum(main.record.cellular{ch,u}.this_OFFresp(s,:)) -
  ...
  main.record.cellular{ch,u}.this_baselinerate(s));
% Calculate ON transientness
main.record.cellular{ch,u}.ONtransientness(s) = ...
  sum(main.record.cellular{ch,u}.this_ONresp...

```

```

(s,6:(6+marker)))/main.record.cellular{ch,u}.sumONresp(s);
    % Calculate OFF transientness
    main.record.cellular{ch,u}.OFFtransientness(s) = ...
        sum(main.record.cellular{ch,u}.this_OFFresp...

(s,1:marker))/(main.record.cellular{ch,u}.sumOFFresp(s));
    % Calculate ON proportionality
    main.record.cellular{ch,u}.ONpropn(s) =....
        main.record.cellular{ch,u}.sumONresp(s)/...
        (main.record.cellular{ch,u}.sumONresp(s)+...
        main.record.cellular{ch,u}.sumOFFresp(s));
    % Calculate ON latency
    [main.record.cellular{ch,u}.peakONval(s), ...
        main.record.cellular{ch,u}.peakONlatency(s)] = ...
        max(main.record.cellular{ch,u}.this_sumPSTH...
        (s, 1:(stimulustime/main.record.global.binsize)));
    % Calculate OFF latency
    [main.record.cellular{ch,u}.peakOFFval(s), ...
        main.record.cellular{ch,u}.peakOFFlatency(s)] = ...
        max(main.record.cellular{ch,u}.this_sumPSTH...
        (s, (stimulustime/main.record.global.binsize):...
        length(main.record.cellular{ch,u}.this_sumPSTH)));
    end % end for s = 1:numstims
    end % end if N1 is not empty
end % end for u
end % end for ch

% END FUNCTION avgRandFF_E.m

%%%%%%%%%%%%%%%%%%%%%%%%%%%%%%%%%%%%%%%%%%%%%%%%%%%%%%%%%%%%%%%%%%%%%%%%
%
% CellSummary.m
%
% Programmer: Erik Nylen, Stasheff Lab, University of Iowa
%
% Inputs:
%   main: all 'main' files of interest are loaded here
%         into a 'summary_cell'
%
% Outputs:
%   summary_cell: structure containing all data for specific
%                 cell types, e.g., wt, rd1, adult
%
%%%%%%%%%%%%%%%%%%%%%%%%%%%%%%%%%%%%%%%%%%%%%%%%%%%%%%%%%%%%%%%%%%%%%%%%
load num_main % # of 'main' files to load, i.e., number of experiments
% using for calculations
for i = 1:num_main
    uiopen('LOAD');
    store_main{1,i} = main;
    clear main;
    pause(.05)
end % end for i = 1:num_main
save store_main store_main;

% pre-allocate structure

```

```

summary_cell(1:1000) = struct('ch', zeros(1,1), 'u', zeros(1,1), ...
    'netONresp', zeros(1,17), 'netOFFresp', zeros(1,17), ...
    'netBOTHresp', zeros(2,17), 'ONpropn', zeros(1,17), ...
    'rate', [], 'baselinerate', zeros(1,17), 'yfitON', ...
    zeros(1,17), 'p_on', zeros(1,4), 'yfitOFF', zeros(1,17), ...
    'p_off', zeros(1,4), 'stimtype', [], 'logtitle', [], ...
    'ONtransientness', zeros(1,17), 'OFFtransientness', ...
    zeros(1,17), 'spiketimes', zeros(1,50000), 'sumPSTH', ...
    zeros(17,106), 'peakONlatency', zeros(1,17), ...
    'peakOFFlatency', zeros(1,17), 'N1', zeros(1,104951));
z = 1;
for i = 1:num_main % cycle through all mains
for ch = 12:87 % cycle through all channels
for u = 1:5 % cycle through all units
    % all relevant values saved into summary_cell
    if (isfield(store_main{1,i}.record.cellular{ch,u}, 'netONresp')...
        &&
~isempty(store_main{1,i}.record.cellular{ch,u}.netONresp))
        summary_cell(z).ch = ch;
        summary_cell(z).u = u;
        summary_cell(z).netONresp = ...
            store_main{1,i}.record.cellular{ch,u}.netONresp;
        summary_cell(z).netOFFresp = ...
            store_main{1,i}.record.cellular{ch,u}.netOFFresp;
        summary_cell(z).netBOTHresp = ...
            [store_main{1,i}.record.cellular{ch,u}.netONresp; ...
            store_main{1,i}.record.cellular{ch,u}.netOFFresp];
        summary_cell(z).ONpropn = ...
            store_main{1,i}.record.cellular{ch,u}.ONpropn;
        summary_cell(z).rate = ...
            [store_main{1,i}.record.cellular{ch,u}.sumONresp/...
            store_main{1,i}.record.global.numtrials; ...
            store_main{1,i}.record.cellular{ch,u}.sumOFFresp/...
            store_main{1,i}.record.global.numtrials];
        summary_cell(z).baselinerate = ...

(max(store_main{1,i}.record.cellular{ch,u}.this_baselinerate))/...
        store_main{1,i}.record.global.numtrials;
        if isfield(store_main{1,i}.record.cellular{ch,u}, 'yfitON')
            summary_cell(z).yfitON = ...
                store_main{1,i}.record.cellular{ch,u}.yfitON;
            summary_cell(z).p_on = ...
                store_main{1,i}.record.cellular{ch,u}.p_on;
        end
        if isfield(store_main{1,i}.record.cellular{ch,u}, 'yfitOFF')
            summary_cell(z).yfitOFF = ...
                store_main{1,i}.record.cellular{ch,u}.yfitOFF;
            summary_cell(z).p_off = ...
                store_main{1,i}.record.cellular{ch,u}.p_off;
        end
        summary_cell(z).stimtype = ...
            store_main{1,i}.record.global.stimtype;
        summary_cell(z).logtitle = ...
            store_main{1,i}.record.global.logtitle;
        summary_cell(z).ONtransientness = ...
            store_main{1,i}.record.cellular{ch,u}.ONtransientness;
        summary_cell(z).OFFtransientness = ...

```

```

        store_main{1,i}.record.cellular{ch,u}.OFFtransientness;
summary_cell(z).spiketimes = ...
        store_main{1,i}.record.cellular{ch,u}.spiketimes;
summary_cell(z).sumPSTH =...
        store_main{1,i}.record.cellular{ch,u}.this_sumPSTH;
summary_cell(z).peakONlatency = ...
        store_main{1,i}.record.cellular{ch,u}.peakONlatency;
summary_cell(z).peakOFFlatency = ...
        store_main{1,i}.record.cellular{ch,u}.peakOFFlatency;
summary_cell(z).N1 = ...
        (store_main{1,i}.record.cellular{ch,u}.N1)';
summary_cell(z).stimONtimes = ...
        store_main{1,i}.record.global.stimON;
summary_cell(z).splicesync = ...
        store_main{1,i}.record.global.logdata.splicesync;
z = z+1;
    end % end if isfield
end % end for u
end % end for ch
end

save summary_cell summary_cell;

% END FUNCTION CellSummary.m

%%%%%%%%%%%%%%%%%%%%%%%%%%%%%%%%%%%%%%%%%%%%%%%%%%%%%%%%%%%%%%%%%%%%%%%%
%
% Plot_Stats.m
%
% Programmer: Erik Nysten, Stasheff Lab, University of Iowa
%
% Inputs:
%   'adult': cell_summary data of adult RGCs
%   'rd1': cell_summary data of rd1 RGCs
%   'wtP14': cell_summary data of wtP14 RGCs 5
%
% Outputs:
%   figures plotting all data for thesis, as plotted shown
%   above in text
%
%%%%%%%%%%%%%%%%%%%%%%%%%%%%%%%%%%%%%%%%%%%%%%%%%%%%%%%%%%%%%%%%%%%%%%%%

% load in data
load adult; load rd1; load wtP14;

% Create strings of character labels equal to data length
for i = 1:length(wtP14)
    wtP14label{i} = 'wtP14';
end
for i = 1:length(adult)
    adultlabel{i} = 'adult';
end
for i = 1:length(rd1)
    rd1label{i} = 'rd1';
end
end

```

```

g=1; % reset counter
for i = 1:length(wtP14)
    % if stimulus type was on an arithmetic scale
    if strcmp(wtP14(i).stimtype, 'arith')
        % if positive slop and I50 is less than 17
        if (wtP14(i).p_on(3) > 0 && wtP14(i).p_on(3) < 17)
            % scale I50 values
            wtP14ONthresh(g) = 17*0.0625*wtP14(i).p_on(3);
            % extract sigmoid model fit
            wtP14ONfit(g,:) = wtP14(i).yfitON;
            % create stimulus value reference array
            wtP14xval(g,:) = [0:1/16:1];
            % extract slope of curve at I50
            wtP14slope(g) = wtP14(i).p_on(4);
            g=g+1;
        end
        % if stimulus type was on a log scale
    elseif strcmp(wtP14(i).stimtype, 'log')
        if (wtP14(i).p_on(3) > 0 && wtP14(i).p_on(3) < 17)
            % scale I50 values
            wtP14ONthresh(g) = 17*10^(2.1251*wtP14(i).p_on(3)/...
                17-2.1251); % I50
            % extract sigmoid model fit
            wtP14ONfit(g,:) = wtP14(i).yfitON;
            % create stimulus value reference array
            wtP14xval(g,:) = logspace(-2,0,17);
            % extract slope of curve at I50
            wtP14slope(g) = wtP14(i).p_on(4);
            g=g+1;
        end
    end
end
end

g=1; % reset counter
for i = 1:length(rd1)
    % if stimulus type was on an arithmetic scale
    if strcmp(rd1(i).stimtype, 'arith')
        % if positive slop and I50 is less than 17
        if ((rd1(i).p_on(3) > 0) && (rd1(i).p_on(3) < 17))
            % scale I50 values
            rd1ONthresh(g) = 17*0.0625*rd1(i).p_on(3);
            % extract sigmoid model fit
            rd1ONfit(g,:) = rd1(i).yfitON;
            % create stimulus value reference array
            rd1xval(g,:) = [0:1/16:1];
            % extract slope of curve at I50
            rd1slope(g) = rd1(i).p_on(4);
            g=g+1;
        end
        % if stimulus type was on a log scale
    elseif strcmp(rd1(i).stimtype, 'log')
        % if positive slop and I50 is less than 17
        if ((rd1(i).p_on(3) > 1) && (rd1(i).p_on(3) < 17))
            % scale I50 values
            rd1ONthresh(g) = 17*10^(2.1251*rd1(i).p_on(3)/...
                17-2.1251);
            % extract sigmoid model fit

```

```

        rd1ONfit(g,:) = rd1(i).yfitON;
        % create stimulus value reference array
        rd1xval(g,:) = logspace(-2,0,17);
        % extract slope of curve at I50
        rd1slope(g) = rd1(i).p_on(4);
        g=g+1;
    end;
end
end

figure % FIGURE 6 IN TEXT
subplot(211)
for g = 1:length(wtP14xval) % for all values
    % plot all IR curves
    plot(wtP14xval(g,:), wtP14ONfit(g,:), 'k');
    hold on
end
proptitle = 'WT P14 Stimulus-Response Sigmoid Fit Curves';
title(proptitle); % set title
ylabel('Normalized Response'); % set labels
xlabel('Relative Intensity');
hold off

subplot(212), % plot histogram of I50 values, 25 bins
wtthreshbar = hist(wtP14ONthresh, 25)/length(wtP14ONthresh);
% plot bar of histogram
bar([min(wtP14ONthresh):(max(wtP14ONthresh)-...
    min(wtP14ONthresh))/24:max(wtP14ONthresh)]...
    , wtthreshbar,'FaceColor','k');
title('I_5_0'); % set title
ylabel('% of Cells'); % set labels
xlabel('Relative Intensity');
xlim([0 17]); % set x scale limits
saveas(gca, proptitle, 'tif'); % save figure

figure % FIGURE 7 IN TEXT
subplot(211)
for g = 1:length(rd1xval)% for all values
    % plot all IR curves
    plot(rd1xval(g,:), rd1ONfit(g,:), 'k');
    hold on
end
hold off
proptitle = 'RD1 P14 Stimulus-Response Sigmoid Fit Curves';
title(proptitle); % set title
xlabel('Relative Intensity'); % set labels
ylabel('Normalized Response');

subplot(212), % plot histogram of I50 values, 25 bins
rd1threshbar = hist(rd1ONthresh, 25)/length(rd1ONthresh);
bar([min(rd1ONthresh):(max(rd1ONthresh)-min(rd1ONthresh))/...
    24:max(rd1ONthresh)], rd1threshbar,'FaceColor','w',...
    'EdgeColor','k','LineWidth',1);
xlim([0 17]); % set x scale limits
ylabel('% of Cells'); % set labels
xlabel('Relative Intensity');
```

```

        title('I_5_0'); % set title
        saveas(gca, proptitle, 'tif'); % save figure

g=1; % reset counter
wtP14ONslopes = [];
wtP14slopetitle = [];
for i = 1:length(wtP14)
    % extract all positive slopes
    if (wtP14(i).p_on(4)>0 && wtP14(i).p_on(4)<100 && ...
        wtP14(i).p_on(3)>0 && wtP14(i).p_on(3) < 20)
        wtP14ONslopes(g) = ([wtP14(i).p_on(4)]);
        wtP14slopetitle{g} = 'wtP14'; % create title string
        g=g+1; % increment
    end
end
g = 1; % reset counter
rd1ONslopes = [];
rd1slopetitle = [];
for i = length(rd1)
    % extract all positive slopes
    if (rd1(i).p_on(4) > 0 && rd1(i).p_on(4) < ...
        100 && rd1(i).p_on(3) > 0 && rd1(i).p_on(3) < 20)
        rd1ONslopes(g) = (rd1(i).p_on(4));
        rd1slopetitle{g} = 'rd1'; % create title string
        g=g+1; % increment
    end
end

% create histograms of slopes
wth = hist(wtP14ONslopes, 25)/length(wtP14ONslopes);
rdh = hist(rd1ONslopes, 25)/length(rd1ONslopes);
% FIGURE 8 IN TEXT
figure, bar([1:25],[wth]', 'BarWidth',.4,'FaceColor','k'),
    hold on % plot wt bar graphs with rd1 data
    bar([1.4:1:25.4],[rdh]', 'BarWidth',.4,'FaceColor','w'),
    hold off
    legend({'Wild Type','RD1'}); % display legend
    disttitle = 'Distribution of Slopes in WT and RD1 at P14';
    xlabel('Slope at I_5_0'); % set labels
    ylabel('% of Cells');
    title(disttitle);
    saveas(gca, disttitle, 'tif'); % save figure

% Perform Kruskal-Wallis test for similarity between groups
[p,tbl,stats] = kruskalwallis([wtP14ONslopes rd1ONslopes],...
    [wtP14slopetitle rd1slopetitle])
[c,m] = multcompare(stats) % p value listed in text

% extract data from structures
wtP14ONpropn = ([wtP14.ONpropn]);
adultONpropn = ([adult.ONpropn]);
rd1ONpropn = ([rd1.ONpropn]);
wtP14RDI = abs((0.5-wtP14ONpropn)/0.5);
rd1RDI = abs((0.5-rd1ONpropn)/0.5);
adultRDI = abs((0.5-adultONpropn)/0.5);
% Perform Kruskal-Wallis test for similarity between groups

```

```

[p,tbl,stats] = kruskalwallis([wtP14RDI([17:17:length(wtP14RDI)]) ...
    rd1RDI([17:17:length(rd1RDI)])],[wtP14label rd1label])
f = figure % only p value reported in text
[c,m] = multcompare(stats)

[p,tbl,stats] = kruskalwallis([wtP14RDI([17:17:length(wtP14RDI)]) ...
    adultRDI([17:17:length(adultRDI)]) ...
    rd1RDI([17:17:length(rd1RDI)])],[wtP14label adultlabel rd1label])
f = figure % plot statistics (only p value shown in text)
[c,m] = multcompare(stats)
h1 = hist(wtP14RDI([17:17:length(wtP14RDI)]), 40)/...
    length([17:17:length(wtP14RDI)]);
h2 = hist(adultRDI([17:17:length(adultRDI)]), 40)/...
    length([17:17:length(adultRDI)]);
h3 = hist(rd1RDI([17:17:length(rd1RDI)]), 40)/...
    length([17:17:length(rd1RDI)]);

% FIGURE 10 IN TEXT
figure, subplot(311), bar([0:1/39:1], h1, 'FaceColor', 'k', ...
    'EdgeColor', 'k', 'LineWidth', 1),
    % plot response dominance for wt
    set(gca, 'YLim', [0 max(h2)], 'XLim', [-0.025 1.025]);
    title('WT P14 Response Dominance Index');
    ylabel('% of Cells'); % set label
subplot(312), bar([0:1/39:1], h3, 'FaceColor', 'w', ...
    'EdgeColor', 'k', 'LineWidth', 1),
    set(gca, 'YLim', [0 max(h2)], 'XLim', [-0.025 1.025]);
    title('RD1 P14 Response Dominance Index');
    ylabel('% of Cells'); % set label
    % plot response dominance for rd1
subplot(313), bar([0:1/39:1], h2, 'FaceColor', [.5 .5 .5], ...
    'EdgeColor', 'k', 'LineWidth', 1),
    set(gca, 'YLim', [0 max(h2)], 'XLim', [-0.025 1.025]);
    title('WT Adult Response Dominance Index');
    ylabel('% of Cells'); % set label
    % plot response dominance for wt adult
proptitle = 'Response Dominance Index';
saveas(gca, proptitle, 'jpg'); % save figure

wtP14peakONlatency = ([wtP14.peakONlatency]);
rd1peakONlatency = ([rd1.peakONlatency]);
% Kruskal-Wallis test to test for differences in ON latency
[p,tbl,stats] = kruskalwallis([wtP14peakONlatency([17:17:...
    length(wtP14peakONlatency)]) rd1peakONlatency([17:17:...
    length(rd1peakONlatency)])],[wtP14label rd1label])
f = figure % plot statistics (only p value shown in text)
[c,m] = multcompare(stats)

hbins = 15; % number of bins for plotting
% create histogram for ON latency in wt
hwt = hist(wtP14peakONlatency([17:17:length(wtP14peakONlatency)]), ...
    hbins)/length(wtP14peakONlatency([17:17:...
    length(wtP14peakONlatency)]));

```

```

% create histogram x values
hwtbar = [0:max(wtP14peakONlatency([17:17:...
    length(wtP14peakONlatency)])))/(length(hwt)-1):...
    max(wtP14peakONlatency([17:17:length(wtP14peakONlatency)]))];
% create histogram x values
hrdbar = [0:max(wtP14peakONlatency([17:17:...
    length(wtP14peakONlatency)])))/(length(hwt)-1):...
    max(rd1peakONlatency([17:17:length(rd1peakONlatency)]))];
% create histogram for ON latency in rd1
hrd = hist(rd1peakONlatency([17:17:length(rd1peakONlatency)]),...
    length(hrdbar)) /length(rd1peakONlatency([17:17:...
    length(rd1peakONlatency)]));

% FIGURE 11 IN TEXT
figure, % plot bar graph of wt and rd1 ON latency
bar((hwtbar+.3), hwt, 'k', 'BarWidth', .4);
hold on, bar((hrdbar+1), hrd, 'w', 'BarWidth', .4),
set(gca, 'XLim', [5 52], 'XTick', [5 15 25 35 45], ...
    'XTickLabel', {'0', '10', '20', '30', '40'});
legend({'Wild Type', 'RD1'});
bartitle = ...
    'Distribution of ON Response Latency for Bright Stimulus in
Retinal Ganglion Cells';
title(bartitle);
ylabel('Number of Cells'); % set label
xlabel('Time (20 ms bins)');
saveas(gca, bartitle, 'bmp'); % save figure

% Now plot statistics for OFF latencies
wtP14peakOFFlatency = ([wtP14.peakOFFlatency]);
rd1peakOFFlatency = ([rd1.peakOFFlatency]);

[p,tbl,stats] = kruskalwallis([wtP14peakOFFlatency([17:17:...
    length(wtP14peakOFFlatency)]) rd1peakOFFlatency([17:17:...
    length(rd1peakOFFlatency)])],[wtP14label rd1label])
f = figure % plot statistics (only p value shown in text)
[c,m] = multcompare(stats)

hbins = 15; % set # of bins for histogram
% create histogram for OFF latency in wt
hwt = hist(wtP14peakOFFlatency([17:17:...
    length(wtP14peakOFFlatency)]), hbins)/...
    length(wtP14peakOFFlatency([17:17:...
    length(wtP14peakOFFlatency)]));
hwtbar = [0:max(wtP14peakOFFlatency([17:17:...
    length(wtP14peakOFFlatency)])))/...
    (length(hwt)-1):max(wtP14peakOFFlatency([17:17:...
    length(wtP14peakOFFlatency)]))];
hrdbar = [0:max(wtP14peakOFFlatency([17:17:...
    length(wtP14peakOFFlatency)])))/...
    (length(hwt)-1):max(rd1peakOFFlatency([17:17:...
    length(rd1peakOFFlatency)]))];
% create histogram for OFF latency in rd1
hrd = hist(rd1peakOFFlatency([17:17:...
    length(rd1peakOFFlatency)]), length(hrdbar))/...
    length(rd1peakOFFlatency([17:17:...

```

```

length(rdlpeakOFFlatency)]));

figure, % FIGURE 13 IN TEXT
bar((hwtbar+.35), hwt, 'k', 'BarWidth', .4);
hold on, bar((hrdbar+1.8), hrd, 'w', 'BarWidth', .4),
set(gca, 'XLim', [0 52], 'XTick', [0 10 20 30 40], ...
    'XTickLabel', {'0', '10', '20', '30', '40'});
legend({'Wild Type', 'RD1'}); % show legend
bartitle = ...
'Distribution of OFF Response Latency for Bright Stimulus in
Retinal Ganglion Cells';
title(bartitle);
ylabel('Number of Cells'); % set labels
xlabel('Time (20 ms bins)');
saveas(gca, bartitle, 'bmp'); % save figure

% extract ON transientness values
wtP14ONtransientness = ([wtP14.ONtransientness]);
rdlONtransientness = ([rdl.ONtransientness]);

% Calculate statistics for transientness at each luminance level
for i = 1:17
lumofinterest = i; % increment luminance level used
% transientness values for all wt cells
wttrans = (wtP14ONtransientness([lumofinterest:17:...
    length(wtP14ONtransientness)]));
% calculate mean transientness in wt
wttransmean(i) = mean(wttrans(~isnan(wttrans)));
% calculate st dev for transientness in wt
wttransstd(i) = std(wttrans(~isnan(wttrans)));
% transientness values for all rd1 cells
rdltrans = (rdlONtransientness([lumofinterest:17:...
    length(rdlONtransientness)]));
% calculate mean transientness in rd1
rdltransmean(i) = mean(rdltrans(~isnan(rdltrans)));
% calculate mean transientness in rd1
rdltransstd(i) = std(rdltrans(~isnan(rdltrans)));
% Kruskal-Wallis test comparing transientness values
[p,tbl,stats] = kruskalwallis([wtP14ONtransientness...
    ([lumofinterest:17:length(wtP14ONtransientness)])...
    rdlONtransientness([lumofinterest:17:...
    length(rdlONtransientness)]),[wtP14label rd1label]) ;
end

figure, % FIGURE 12 IN TEXT
plot(wttransmean, 'k', 'LineWidth', 2), hold on,
    plot(rdltransmean, 'k', 'LineStyle', ':', 'LineWidth', 2)
set(gca, 'XTick', [1:2:17], 'XTickLabel', [0:2:16])
ptitle = ...
'ON Transientness at Increasing Luminance Stimulation';
title(ptitle);
xlabel('Relative Luminance');
ylabel('Transientness');
legend({'Mean WT P14', 'Mean RD1 P14'});
saveas(gca, ptitle, 'bmp');

```

```

figure, subplot(311), hist(wtP14ONtransientness([17:17:...
    length(wtP14ONtransientness)]))
subplot(312), hist(adultONtransientness([17:17:...
    length(adultONtransientness)]))
subplot(313), hist(rd1ONtransientness([17:17:...
    length(rd1ONtransientness)]))

wtP14baselinerate = ([wtP14.baselinerate]);
rd1baselinerate = ([rd1.baselinerate]);

[p,tbl,stats] = kruskalwallis([wtP14baselinerate ...
    rd1baselinerate],[wtP14label rd1label])
f = figure, % statistics for baseline rate, only p value shown in text
    [c,m] = multcompare(stats)
xc = [0:1:50];
hwt = hist(wtP14baselinerate, xc)/length(wtP14baselinerate);
hrd = hist(rd1baselinerate, xc)/length(rd1baselinerate);

figure, % FIGURE 4 IN TEXT
    bar(xc+.15, hwt, 'k', 'BarWidth', .4); hold on,
    bar(xc+.4, hrd, 'w', 'BarWidth', .4),
        set(gca, 'XLim', [0 20]);
    legend({'Wild Type', 'RD1'});
    bartitle = ...
'Distribution of Spontaneous Spike Activity in Retinal Ganglion
Cells';
    title(bartitle);
    ylabel('Number of Cells');
    xlabel('Spontaneous Firing Rate (spikes/s)');
    saveas(gca, bartitle, 'bmp');

wtP14rate = ([wtP14.rate]);
rd1rate = ([rd1.rate]);
lumofinterest = 17; % HIGHEST STIMULUS INTENSITY
[p,tbl,stats] = kruskalwallis([wtP14rate(1,[lumofinterest:17:...
    length(wtP14rate)])...
    rd1rate(1,[lumofinterest:17:length(rd1rate)])],...
    [wtP14label rd1label])
f = figure,
    [c,m] = multcompare(stats)
proptitle = 'Firing rate with stimulus at highest intensity';
title(gca, proptitle);
saveas(gca, proptitle, 'jpg');

% compare adult to rd1
lumofinterest = 17;
[p,tbl,stats] = kruskalwallis([adultrate(1,[lumofinterest:17:...
    length(adultrate)])...
    rd1rate(1,[lumofinterest:17:length(rd1rate)])],...
    [adultrate rd1label])
f = figure, % calculate statistics, only p value shown in text
[c,m] = multcompare(stats)

```

```

hwtrate = hist(wtP14rate(1,[lumofinterest:17:...
    length(wtP14rate)]), 25)/length(wtP14rate(1,...
    [lumofinterest:17:length(wtP14rate)]));
hwtratebar = [0:max(wtP14rate(1,[lumofinterest:17:...
    length(wtP14rate)]))/(length(hwtrate)-1):max(wtP14rate(1,...
    [lumofinterest:17:length(wtP14rate)]))];
hrdratebar = [0:max(wtP14rate(1,[lumofinterest:17:...
    length(wtP14rate)]))/(length(hwtrate)-1):max(rd1rate(1,...
    [lumofinterest:17:length(rd1rate)]))];
hrdrate = hist(rd1rate(1,[lumofinterest:17:...
    length(rd1rate)]), length(hrdratebar))/...
    length(rd1rate(1,[lumofinterest:17:length(rd1rate)]));

figure, % FIGURE 5 IN TEXT
bar(hwtratebar+2), hwtrate, 'k', 'BarWidth', .4);
hold on, bar(hrdratebar+4.5), hrdrate, 'w', 'BarWidth', .4),
set(gca, 'XLim', [0 150]);
legend({'Wild Type', 'RD1'});
bartitle = ...
'Distribution of Responses to Bright Stimulus in Retinal Ganglion
Cells';
title(bartitle);
ylabel('Number of Cells');
xlabel('Response Rate (spikes/s)');
saveas(gca, bartitle, 'bmp');

for i = 1:length(wtP14)
    wtP14(i).cumN = nonzeros([wtP14(1:i).N1]);
end
for i = 1:length(wtP14)
    wtP14(i).logN = -1*sum((nonzeros(wtP14(i).cumN)./...
        sum((wtP14(i).cumN))).*log(nonzeros(wtP14(i).cumN)./...
        sum((wtP14(i).cumN))));
    wtP14(i).indN = -1*sum((nonzeros(wtP14(i).N1)./...
        sum((wtP14(i).N1))).*log(nonzeros(wtP14(i).N1)./...
        sum((wtP14(i).N1))));
end
[hwtN, hwtNx] = hist([wtP14.indN]);

for i = 1:length(rd1)
    rd1(i).cumN = nonzeros([rd1(1:i).N1]);
end
for i = 1:length(rd1)
    rd1(i).logN = -1*sum((nonzeros(rd1(i).cumN)./...
        sum((rd1(i).cumN))).*log(nonzeros(rd1(i).cumN)./...
        sum((rd1(i).cumN))));
    rd1(i).indN = -1*sum((nonzeros(rd1(i).N1)./...
        sum((rd1(i).N1))).*log(nonzeros(rd1(i).N1)./...
        sum((rd1(i).N1))));
end
[hrd1N, hrd1Nx] = hist([rd1.indN]);

figure, % FIGURE 15 IN TEXT
bar(hwtNx, hwtN/sum(hwtN), 'BarWidth', .5, 'FaceColor', 'k', ...

```

```

        'LineWidth',.5), hold on,
bar(hrd1Nx+.55, hrd1N/sum(hrd1N), 'BarWidth',.5,...
    'FaceColor','w','LineWidth',.5);
legend({'WT P14','RD1 P14'});
xlabel('Naive Entropy');
ylabel('% of Cells');
    ptitle = 'Distribution of Naive Entropy Estimates';
title(ptitle);
saveas(gca, ptitle, 'jpg');

[p,tbl,stats] = kruskalwallis([([wtP14.indN]) ...
    ([rd1.indN]),[wtP14label rd1label])
f = figure % calculate statistics, only p value shown in text
[c,m] = multcompare(stats)

% Now, find noise entropy and mutual information entropies here.
vect50 = 0:1:49;
% splicesync data lists ON stimulus times, in bin #
for i = 1:length(wtP14)
    stimuse = length(nonzeros(min(wtP14(i).stimONtimes)));
    % useable number of stims
    square50 = repmat(vect50,stimuse,1);
    for s = 1:17
        holdmat = repmat(wtP14(i).splicesync(wtP14(i).stimONtimes(s,...
            1:stimuse)),1,50)+square50;
        wtNs(i,s).Nvals = wtP14(i).N1(holdmat);
        wtNs(i,s).ent = -1*sum((nonzeros(wtNs(i,s).Nvals)./...
            sum(sum((wtNs(i,s).Nvals))))).*log(nonzeros(wtNs(i,...
            s).Nvals)./sum(sum((wtNs(i,s).Nvals)))));
        wtentscantemp(i,s) = wtNs(i,s).ent;
    end % end for s
    wtentband(i) = max(wtentscantemp(i,:))-min(wtentscantemp(i,:));
    wtminent(i) = min(wtentscantemp(i,:));
end

for i = 1:length(rd1)
    stimuse = length(nonzeros(min(rd1(i).stimONtimes)));
    % useable number of stims
    square50 = repmat(vect50,stimuse,1);
    for s = 1:17
        holdmat = repmat(rd1(i).splicesync(rd1(i).stimONtimes(s,...
            1:stimuse)),1,50)+square50;
        rd1Ns(i,s).Nvals = rd1(i).N1(holdmat);
        rd1Ns(i,s).ent = -1*sum((nonzeros(rd1Ns(i,s).Nvals)./...
            sum(sum((rd1Ns(i,s).Nvals))))).*...
            log(nonzeros(rd1Ns(i,s).Nvals)./sum(sum((rd1Ns(i,...
            s).Nvals)))));
        rd1entscantemp(i,s) = rd1Ns(i,s).ent;
    end % end for s
    rd1entband(i) = max(rd1entscantemp(i,:))-min(rd1entscantemp(i,:));
    rd1minent(i) = min(rd1entscantemp(i,:));
end
xc = [0:.5:10];
hwtent = hist(wtentband,xc);
hrd1ent = hist(rd1entband,xc);

```

```

figure, % FIGURE 17 IN TEXT
    bar(xc+.5, hwtent/sum(hwtent), 'FaceColor','k','BarWidth',.5),
        hold on,
    bar(xc+.75, hrdlent/sum(hrdlent), 'FaceColor','w','BarWidth',.5)
set(gca, 'XLim',[0 7]);
xlabel('Maximum Mutual Information');
ylabel('% of Cells');
    ptitle = 'Distribution of Optimal Entropies';
legend({'WT P14','RD1 P14'});
title(ptitle);
saveas(gca, ptitle, 'jpg');

hwtminent = hist(wtminent, xc);
hrdlminent = hist(rdlminent, xc);

figure, % FIGURE 16 IN TEXT
    bar(xc+.5, hwtminent/sum(hwtminent), 'FaceColor','k',...
        'BarWidth',.5), hold on,
    bar(xc+.75, hrdlminent/sum(hrdlminent),...
        'FaceColor','w','BarWidth',.5)
set(gca, 'XLim',[0 7]);
xlabel('Minimum Noise Entropy');
ylabel('% of Cells');
    ptitle = 'Distribution of Noise Entropies';
legend({'WT P14','RD1 P14'});
title(ptitle);
saveas(gca, ptitle, 'jpg');

[p,tbl,stats] = kruskalwallis([wtentband rdlentband],...
    [wtP14label rdllabel])
f = figure % calculate statistics, only p value shown in text
[c,m] = multcompare(stats)

[p,tbl,stats] = kruskalwallis([wtminent rdlminent],...
    [wtP14label rdllabel])
f = figure % calculate statistics, only p value shown in text
[c,m] = multcompare(stats)
% END FUNCTION Plot_Stats.m

```